Measurement of Carbon Monoxide Production in Atmospheric Pressure Plasmas

Bachelor Thesis
in the Degree Program "Bachelor of Science" in Physics
at the Faculty of Physics and Astronomy of the Ruhr-Universität Bochum

by Daniel Henze

from
Essen

Bochum 2022

1st reviewer: Jun.-Prof. Dr. Judith Golda
2nd reviewer: Dr. Laura Chauvet

Abstract english

The application of minor doses of CO in medical treatment promises a wide range of beneficial therapeutic effects. By using mass spectrometry, the absolute densities of the species produced by the dissociation of CO_2 inside an atmospheric pressure helium plasma jet are measured. The dependency of the CO_2, CO, O and O_2 densities on both the CO_2 admixture and the power injected into the plasma is investigated inside a helium atmosphere and in ambient air. By comparing the results from ambient air with those from the helium atmosphere it was demonstrated that, with the use of threshold ionization mass spectrometry it is possible to measure CO in open air and that measuring in ambient air shows no significant difference from measuring inside the helium atmosphere. Lastly the mass spectrometry results were compared with results obtained via gas analysis, showing that the measurements are consistent within the same order of magnitude in terms of density by a factor of three and in their behavior when varying both the power and admixture.

Abstract german

Die Benutzung kleiner Mengen an Kohlenstoffmonoxid verspricht eine Vielzahl an positiven Wirkungen in der medizinischen Behandlung. Mittels Massenspektrometrie wurden die absoluten Dichten der an der Produktion von CO, durch Dissoziation von CO_2, teilnehmenden Spezies innerhalb eines atmosphärendruck Helium Plasma Jets gemessen. Die Abhängigkeit der CO_2, CO, O und O_2 Dichten von sowohl der CO_2 Beimischung, als auch der Leistung wurden innerhalb einer künstlichen Helium Atmosphäre und in der Umgebungsluft untersucht. Durch den Vergleich dieser Messungen wurde neben der Tatsache, dass sich CO mittels *threshold ionization mass spectrometry* auch in der Umgebungsluft messen lässt auch gezeigt, dass Messungen in Umgebungsluft keine bedeutsamen Unterschiede zu den Messungen innerhalb der Helium Atmosphäre aufweisen. Letztlich wurde ein Vergleich zwichen den Ergebnissen aus der Massenspektrometrie mit Ergebnissen, die mittels eines Gas Analysators gewonnen wurden, verglichen. Es wurde gezeigt, dass die absoluten Dichten innerhalb der selben Größenordnung konsistent um einen Faktor drei abweichen und das selbe Verhalten bei Variation von Plasmaleistung und CO_2 Beimischung aufweisen.

Contents

1. Introduction

While carbon monoxide (CO) is widely considered toxic and detrimental to health, studies also highlighted its possible use in medical application due to its positive properties in disease treatment when delivered in small doses[1], where it exhibits a variety of benefits such as anti-inflammatory, antiaoptic, antiproliferative and other cell protective effects[2]. With the use of low temperature non-equilibrium plasmas, carbon monoxide is produced by dissociating carbon dioxide (CO_2) thus decreasing the potential health hazard with storing large amounts of CO. The use of low temperature plasmas in medical applications is not unheard of, in fact its potential led to the creation of a whole new research branch known as Plasma Medicine. One of the biggest perks of using a low temperature non-equilibrium plasma is the fact, that the plasma will not burn living tissue. This allows the application of direct and local treatment methods which in the case of CO treatment could supersede the more challenging methods used so far like CO-Inhalation and the use of CO-releasing molecules.
The aim of this thesis is to characterize the cabability of such a plasma in the production of CO from CO_2 in ambient air. For this purpose, helium (He) will act as the carrier gas. The He-CO_2-mixture will be ignited inside the COST reference microplasma jet, since this source is both well characterized and suitable for use in a medical environment, because of its small size and its use of medically certified materials[3].
The main diagnostic will be mass spectrometry supplemented by optical emission spectroscopy.

2. Theory

2.1. Non-equilibrium atmospheric pressure plasma

2.1.1. Fundamentals

A plasma is a partially or completely ionized gas, which shows both collective behaviour and quasi neutrality. The latter means that the density of positive charges is equal to the density of negative charges in that area of quasi neutrality while the former can be understood as the ability to react to changes inside the plasma due to external influences. If for example there was an external electric field, the plasma would counteract it by creating small opposing fields inside of itself.
To evaluate whether or not these conditions are met, there are three parameters which must be satisfied:

- $L > \lambda_D$
  The size of the plasma must be greater than its Debye-Length λ_D in order to screen internal electrical fields that would interfere with quasi neutrality

- $N_D >> 1$
  The number of particles inside of the debye-sphere (sphere with radius λ_D) must be significantly larger than one to ensure collective behavior

- $\omega >> 1/\tau$
  The plasma frequency is much larger than the frequency of electron-neutral particle collisions, so that electrostatic interactions dominate regular gas kinetics

Plasma itself can be further categorized in regard to its parameters. In industrial and technological application the most common categorization is temperature and pressure. In this thesis we will exclusively deal with non-equilibrium atmospheric pressure plasma. The term non-equilibrium refers to the fact, that the electrons inside the plasma have high temperatures of several electron volts (eV), whereas ions and neutral particles have significantly lower temperatures. This leads to non-equilibrium plasma being investigated in medicine, since direct contact with this plasma will not cause burn damage.

2.1.2. Atmospheric pressure jet discharge

In its most basic form the term plasma jet refers to a plasma generated inside a device, with either the plasma itself, or its effluent propagating outside the device. The effluent can be especially important, since its investigation does not cause any change in the plasma.

There are a wide range of plasma jets existing, which can be classified by its parameters [4]. This includes:

- the geometry of the discharge, the arrangement of its electrodes and the configuration of the field
- the type of the generated plasma
- the excitation frequency(e.g. direct current, alternating current,RF-driven)
- The gas composition

The COST-Jet (the technical aspect will be further discussed in Chapter 3) which will be the focus of this thesis is a capacitively coupled radio-frequency discharge.
The ignition of the plasma is achieved by the breakdown of the carrier gas. This breakdown is reached when electron producing processes dominate electron loosing processes. As the applied voltage increases, electrons are accelerated towards the higher potential and thus gain energy. If the voltage is sufficiently high, the electrons will have enough energy to ionize atoms or molecules, leading to an increase in electron density. Repeating this pattern, an electron avalanche is created that can sustain the discharge. For a discharge with electrode distance d, the criterion for the independent ignition is as follows:

$$\alpha d = ln(1 + \frac{1}{\gamma}) \tag{1}$$

where α and γ represent the first and second townsend coefficient respectively. α is characterized by the probability for ionization per mean free path of the electrons, whereas γ is dependant of the materials chosen for the electrodes.
In addition to that, there is the process of secondary electron emission, where electrons are released by the ions hitting the cathode.
The voltage corresponding to the point where breakdown is achieved is called ignition voltage. The relation between the ignition voltage and the parameters of the setup is called the paschen curve (See figure 1a). For a higher pressure environment, where the product of the pressure p and the distance of the electrodes exceeds 10 Torr cm, the relation between ignition Voltage and the aforementioned product becomes proportional: $V \propto pd$. In the case of the COST-Jet the electrodes have a gap of $d = 0.1\,\mathrm{cm}$ and the

pressure is roughly $p \approx 760$ Torr (atmospheric pressure), so the ignition voltage would sit at around 200 V for pure Helium (See figure 1b).

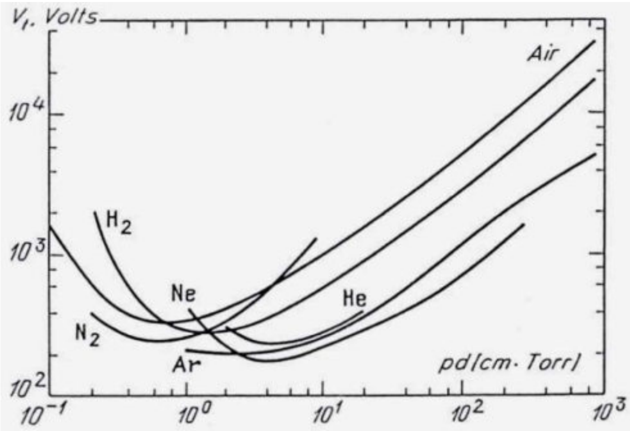

(a)

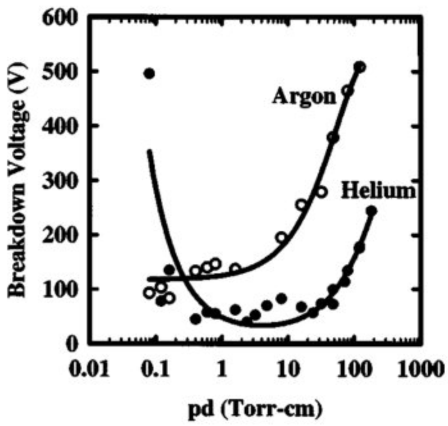

(b)

Figure 1: (a) Paschen curve of low temperature plasmas. (b) Paschen Curve of RF-discharges.[5], [6]

The difference between the classic Paschen Curve figure 1a and the RF-discharge Paschen Curve figure 1b is due to the RF-breakdown mechanism being governed by electrons.

2.2. CO_2-chemistry

The dissociation of CO_2 into CO has been studied extensively by Fridman [7]. The following section will briefly present the basics of the CO_2-chemistry.

$$CO_2 + e^- \rightarrow CO + O + e^- \tag{2}$$

As the atomic oxygen is highly reactive it will quickly react or recombine, so that equation 2 can be summarized to:

$$CO_2 \rightarrow CO + \frac{1}{2}O_2 \tag{3}$$

This represents the chemical equation for the dissociation of CO_2.
The most effective channel for this reaction is through the vibrational excitation of CO_2, because a major portion of the discharge energy is transferred from the electrons to CO_2 vibration, all the while vibrational energy losses are relatively slow.
There are a myriad of ways to dissociate CO_2. The most straightforward approach would be the adiabatic dissociation leading to the creation of electronically excited atomic

oxygen:

$$CO_2^*(^1\Sigma^+) \rightarrow CO(^1\Sigma^+) + O(^1D) \tag{4}$$

This process requires more than 7 eV. The more effective way is the non-adiabatic transition $^1\Sigma \rightarrow {}^3B_2$ by step-by-step vibrational excitation:

$$CO_2^*(^1\Sigma^+) \rightarrow CO_2^*(^3B_2) \rightarrow CO(^1\Sigma^+) + O(^3P) \tag{5}$$

This way of dissociation requires an energy of 5.5 eV, resulting in this process being dominant in the vibrational excitation of CO_2. Subsequently the atomic oxygen can then participate in a secondary reaction with another excited CO_2 molecule to create another CO molecule and molecular oxygen:

$$O + CO_2^* \rightarrow CO + O_2 \tag{6}$$

This process is faster than three-body recombination of atomic oxygen leading to the creation of another CO molecule per dissociation event (Provided the vibrational temperature is above 0.1 eV).
Another method of CO_2 dissociation is through the electronic excitation of molecules. In the presence of very high energy electrons, a significant amount of dissociation events can be attributed to the following process:

$$e^- + CO_2(^1\Sigma^+) \rightarrow CO(a^3\Pi) + O(^3P) \tag{7}$$

This can also be a dominant process provided that there is a high reduced electric field $\frac{E}{p}$, although this does not apply in the setup used during this study.
The last process highlighted here is the attachment of electrons,

$$e^- + CO_2 \rightarrow CO + O^-, \tag{8}$$

which despite of its overall low cross sections is essential in sustaining non-equilibrium discharges in CO_2 and thus worth mentioning.

2.3. Mass spectrometry

Mass spectrometry provides the ability to measure the mass-to charge-ratio m/z of both atoms and molecules and subsequently enables one to compute the absolute densities and relative concentrations of gas mixtures.

There are four main components that every mass spectrometer has:

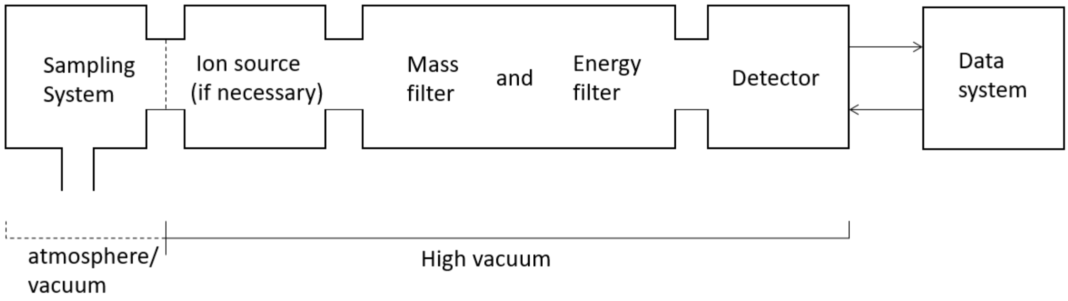

Figure 2: General Scheme of a mass spectrometer. Adapted from [8]

All of these components, except for the sampling system, are operated in a low pressure environment to avoid particle collision inside the mass spectrometer and damage to the equipment.

The main challenge in performing mass spectrometry under atmospheric pressure is overcoming the difference between the high pressure outside and the low pressure inside of the mass spectrometer. To solve this problem, three differential pumping stages that gradually decrease the pressure are utilized. For the regions of the mass spectrometer where ions are created, a low pressure is needed so that the mean free path of the ions is large enough to ensure that they are guided through the mass spectrometer without collision. For the detector an even lower pressure (10^{-6} mbar) is necessary, since this setup uses a secondary electron multiplier (SEM). As such it needs high voltage to operate (∼2 kV) which under sufficiently high pressure will lead to the ignition of of parasitic plasma discharges inside the detector itself, not to mention that with high amounts of electrons hitting the first dynode, the degradation of the detector is rapidly accelerated.

In the following the main components of the mass spectrometer used during the course of this thesis are briefly explored.

2.3.1. Sampling system

Sampling a gas mixture inevitably leads to a distortion in its composition. There are several ways to minimize this effect. In this case, molecular beam sampling is used. This has been thoroughly described by Große-Kreul [9], so it will be summarized here in a concise manner.

A small orifice (usually around tens of μm to 100 μm) serves as an interface between the atmospheric pressure region and the low pressure region. Consequently there is a large

pressure gradient perpendicular to the orifice, which forces the gas particles through a small volume resulting in a supersonic expansion into the low pressure region, thus creating a molecular beam. The geometry of the mass spectrometer must be set up, so that all of the components are aligned to the axis that the molecular beam expands along. Since little to no particle collisions occur after the formation of the molecular beam, both radical and excited species can be measured.
Several effects have to be kept in mind:

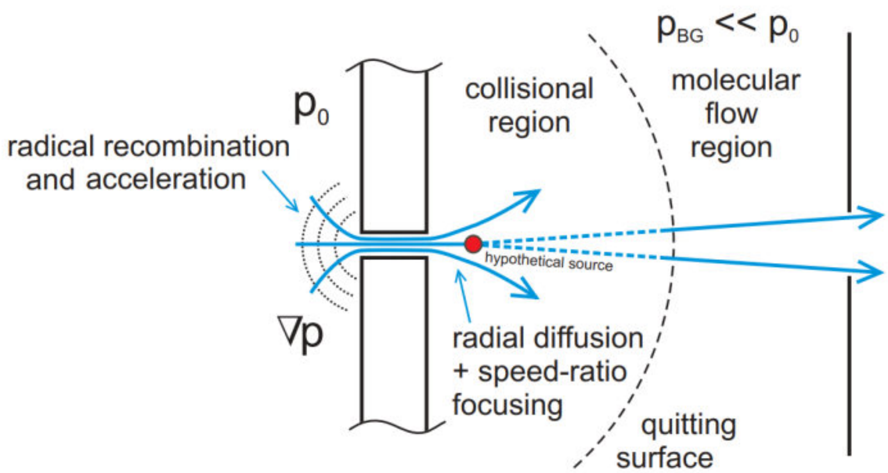

Figure 3: Overview of the effects of molecular beam sampling.
Adapted from [9]
.

1. *Radical recombination:* The Interaction and Recombination between reactive species and the walls of the orifice.

2. *Acceleration into the orifice:* Acceleration due to the high pressure gradient leading to most of measured gas stemming from two to five orifice diameters above the surface

3. *Radial diffusion:* Radial pressure gradients cause a mass seperation through diffusion downstream from the orifice.

4. *Speed-ratio focusing:* While the velocity parallel to the beam is the same for all species, as mentioned before, the perpendicular velocity is strongly dependent on the molecular weight. Thus the speed ratio between parallel and perpendicular velocity is different for particles of different masses.

2.3.2. Ionization source

Because most of the particles arriving in the mass spectrometer carry no charge, they must first be ionized in order for the mass filter to work. The ionization source works by heating a filament to the point where thermionic emission occurs. The emitted electrons are then accelerated by two electrodes until they have reached a set electron energy. Typically this energy is at around 70 eV since the electron impact ionization cross-section of most species is around 70 eV. Though in some cases a lower energy can be beneficial. It should be pointed out however, that the energy distribution of the electrons will behave like a gaussian curve, so not all of the electrons will have the exact same energy. Additionally the filament based ionizer has a certain extraction efficiency depending on the energy that is chosen for the measurement.

2.3.3. Mass filter

The now charged particles must first be separated according to their m/z ratio. There are several ways this can be achieved, be it by Time-of-flight instruments that compare the travel time of a particle to a known kinetic energy, or Sector field instruments that create a spatial separation by applying magnetic or electric fields. In this case, a quadrupole

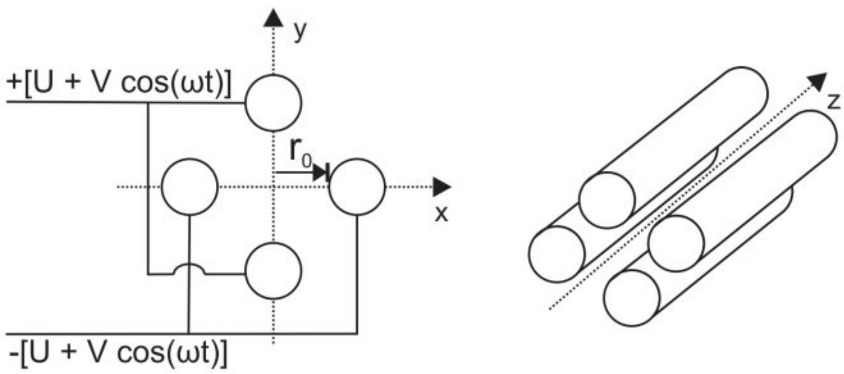

Figure 4: Scheme of a QMA.[10]

mass analyzer (QMA) is used (figure 4). It consist of four metal rods to which electrical potentials with added constant and alternative voltage components are applied.
Through the Coulomb force, charged particles are then accelerated along the oscillating electric field creating a helical trajectory. Depending on the m/z ratio of the species passing through the QMA, this trajectory is either stable or unstable. The particles following an unstable trajectory either recombine with the metal rods, or leave the QMA

entirely. The measured m/z ratio is dependent on the parameters set for the voltages. The QMA has a mass dependent transmission function resulting in a higher intensity for lighter ions than for heavier ones.

2.3.4. Detector

For the detector, a secondary electron multiplier (SEM) is used. It consists of multiple dynodes as seen in figure 5. The first of which is negatively biased to accelerate the ions towards itself. Through secondary emission, electrons are then emitted that are subsequently accelerated towards the second dynode by a positive voltage, releasing more electrons upon impact. This process repeats through all of the dynodes that have successively larger positive voltages than their predecessors to accelerate the electrons throughout the SEM. At the end of the detector the number of electrons will be sufficiently large (10^6-10^8, [10]) to measure a current. The sensitivity of the detector is dependent on the m/z ratio.

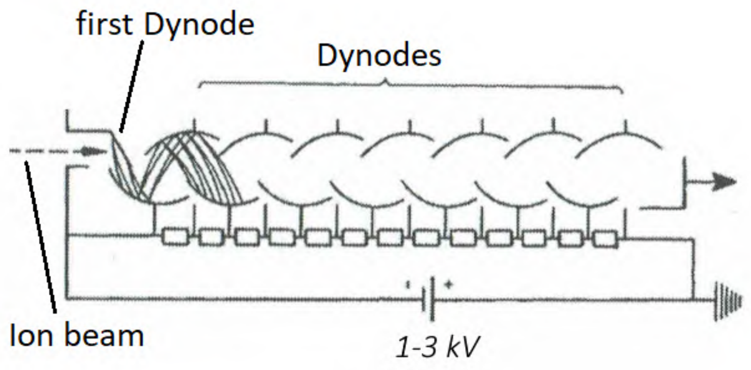

Figure 5: Illustration of an SEM. Adapted from [11]

2.3.5. Absolute densities

The calibration of the signal is discussed at length by Willems [10], but it will be described here in short. Due to the several effects linked to the aforementioned components of the mass spectrometer, there is a discrepancy between the sampled gas at the orifice and the measured gas that has traveled through the mass spectrometer, that must be taken into account. The relation of the output signal S_i of the mass spectrometer and the density

n_i^{gas} of the sampled gas can be seen in equation 9.

$$S_i = n_i^{gas} \cdot CD_i \cdot \sigma_i(EE) \cdot f_i(m_i) \cdot \beta \cdot l_{ionizer} \cdot I_e \tag{9}$$

The effects of composition distortion, discussed in section 2.3.1, is taken into account by the factor CD_i, the transmission functions of both the QMA and the SEM are combined into the generalized transmission function f_i and the cross section for electron impact ionization $\sigma_i(EE)$ is considered. The constants β, $l_{ionizer}$ and I_e correspond to the ion extraction efficiency, the ionizer length and the filaments emission current respectively. By measuring the known density of a calibration gas, the sampled gas density can be calculated using equation 10.

$$n_i^{gas} = n_{cal}^{gas} \cdot \frac{S_i}{S_{cal}} \cdot \frac{CD_{cal}}{CD_i} \cdot \frac{\sigma_{cal}(EE)}{\sigma_i(EE)} \cdot \frac{f_{cal}(m_{cal}}{f_i(m_i)} \tag{10}$$

By linearly fitting the known gas density of the calibration gas to the signal acquired with the mass spectrometer and assuming that $S_{cal} = \alpha \cdot n_{cal}^{gas} + \beta \approx \alpha \cdot n_{cal}^{gas}$, equation 11 is obtained.

$$n_i^{gas} = \frac{S_i}{\alpha} \cdot \frac{\sigma_{cal}(EE) \cdot f_{cal}(m_{cal})}{\sigma_i(EE) \cdot f_i(m_i)} \tag{11}$$

Similar to the work by Willems [10], it was also assumed that the composition distortion factor is equal for both the sampled and the calibration gas. Benedikt et al were able to conclude that $f_i(m_i) = m_i^{-0.88}$ [12].

Ideally the same gas should be used for both measurement and calibration. Because this is often impossible, a gas similar in both mass and adiabatic properties should be chosen. An overview over the measured gas species and their respective calibration gases, as well as the cross sections used, can be found in Appendix B. Calibration should be done on each measurement day to take changes in the mass spectrometer system, especially the degradation of the SEM, into account.

2.3.6. Threshold ionization mass spectrometry

Threshold Ionization Mass Spectrometry (TIMS) utilizes the fact that different reactions have different threshold energies that have to be reached so that they can occur. It consequently enables the suppression of reactions with higher energy thresholds inside of the ionizer. In practice it is often used to discriminate the appearance of dissociatively ionized species. Taking the CO measurements as an example, this prevents the overestimation of the CO produced in the plasma by suppressing the dissociation of CO_2 in the ionizer.

2.4. Optical emission spectroscopy

While mass spectrometry allows one to take an in depth look at absolute densities of the species of interest, the investigation into excited species while possible can be complicated according to the accuracy of the measurements. Optical emission spectroscopy (OES) offers a way to not only look at these excited species more easily, but also create a quick overview of the species, that are generated inside the plasma (that radiatively emit light in the range accessible by OES). With mass spectrometry, although a mass scan over all masses is possible, analyzing the resulting spectrum can be tedious, since what is actually measured is the m/z ratio. This can make the identification of the peaks within the mass spectrum hard, not to mention, that with mass spectrometry there is no distinction between molecules of the same mass, further complicating identification.
OES works by channeling light through an optical cable aimed at the light source (in this case the plasma) and measuring the intensity of the wavelength that make up said light. At the end of the optical fiber there is the actual spectrometer. The spectrometer consist of an optical system and a detector. The optical system most commonly consist of a system of mirrors, that guide the incoming light towards either a prism or a grating, which separates the different wavelengths. Usually a CCD-camera is used for detection of the wavelengths.
The result is a spectrum consisting of both discrete lines which stem from the deexcitation of atoms, and broader band structures, which stem from the deexcitation of molecules, since they can be excited both vibrationally and rotationally. When deexciting from vibrational or rotational energy levels, broader band like structures are often created rather than sharply defined peaks.

3. Experimental setup and methods

3.1. COST-jet

As discussed previously the plasma source of interest will be the COST-reference microplasma jet, because it is straightforward to operate, allows one to easily replicate the conditions of another experiment and it is suitable for medical application since the materials its made of are medically certified. Considering the COST-jet has already been fully described in another study [3], it will not be described in full detail. In this study, the jet was operated with a helium flow of 1 slm with CO_2 admixtures ranging from 0 ppm to 6000 ppm.

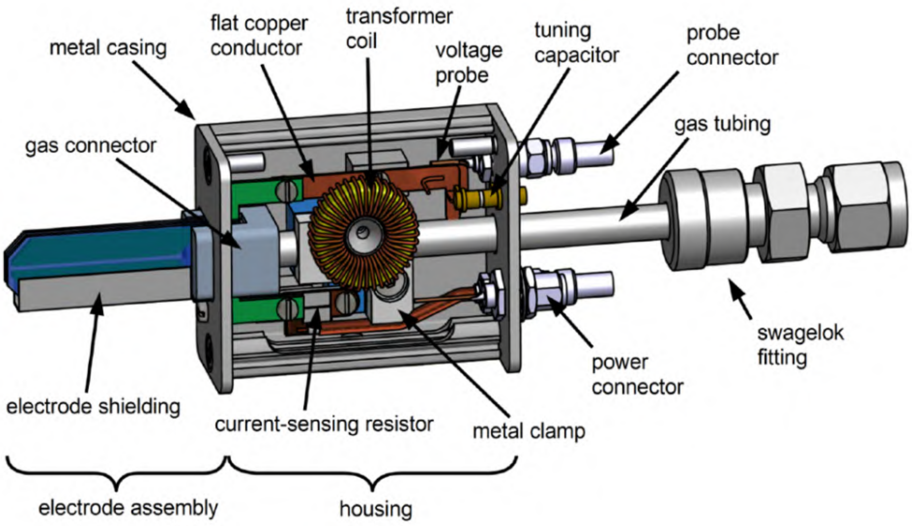

Figure 6: Overview of the COST-jets components.[3]

3.1.1. Plasma source

As seen above, the COST-Jet is essentially a resonant circuit connected to two symmetric electrodes which are 1 mm apart from each other. One of those two electrode remains grounded, while the other is powered by a 13,56 MHz Signal generated by the power supply. The resonant circuit acts as a replacement for an external matchbox, although the capacitor must be tuned during the setup of the experiment.
When connecting the voltage and the current probe to an oscilloscope, 50 Ω terminations should be used to avoid a reflection of the signal.

3.1.2. electrical measurements

Before attempting any experiment, the voltage probe must be calibrated. This can be done by connecting an external commercial voltage probe to the voltage electrode of the jet and linearly fitting the internal voltage to the external voltage. The resulting slope of that fit is the calibration factor for the internal voltage probe. The discharge current can be calculated by measuring the voltage drop over the internal resistor $R_m = 4,7\,\Omega$ using the current probe. With Ohm's law, it follows that:

$$I = U_c \frac{R_m + R_t}{R_m R_t} \tag{12}$$

Where R_t is the resistance of the terminations used on the oscilloscope (50 Ω) and U_c is the voltage that drops over the internal resistor.
To calculate the power that is dissipated into the plasma both the current and the voltage must be measured, in addition to the phase shift in between the two.
The power is then given by:

$$P = U \cdot I \cdot cos(\Phi) \tag{13}$$

All measurements of the voltage, current and power were done using the open source software "COST-power-monitor".

3.1.3. Heating

A heating time of 30 minutes will suffice to create reproducible results (see figure 29, Appendix A). A consequence of this long waiting time is that all measurements with the discharge turned off have to be taken either before or after all measurements with the plasma on. Ideally these should be done right after each measurement so that the most accurate signal can be captured. In this case, the measurements with the discharged turned off are measured both before and after all of the measurements with the turned on discharge.

3.2. Mass spectrometer

3.2.1. Overview

The mass spectrometer used during this thesis is specifically designed to measure neutral species. Its design is illustrated in figure 7.

An orifice with a 100 μm diameter is used to maximize the possible signal whilst still

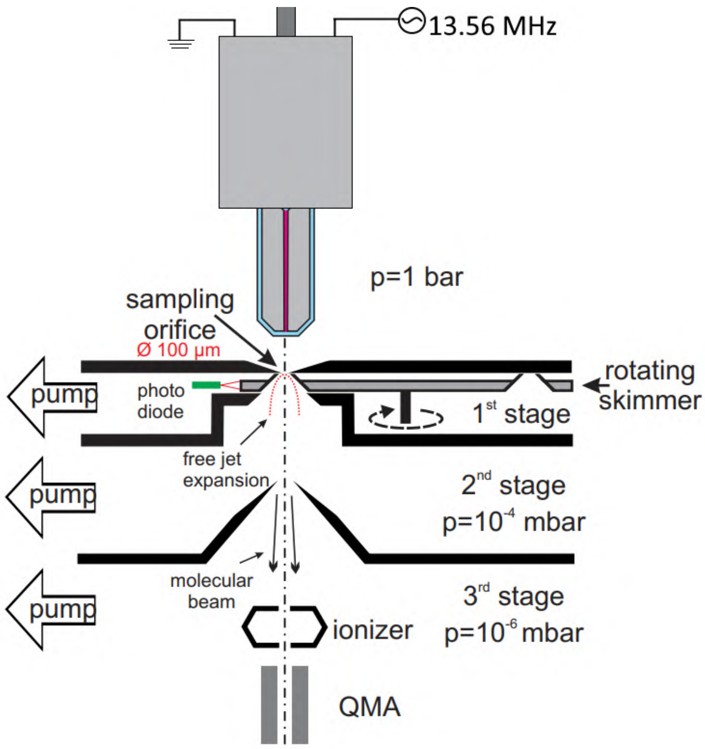

Figure 7: Sketch of the neutral mass spectrometer setup. Adapted from [10]

operating under a safe pressure for the mass spectrometer. As mentioned in in the Theory section, three differential pumping stages are used to gradually lower the pressure.
A special feature of this setup is the use of a chopper. It is mounted right after the sampling orifice. The chopper has four small holes, meaning that while rotating, the chopper remains closed for 98.5 % of the time consequently leading to most of the measured signal originating from the small background inside of the housing of the mass spectrometer, while the gas coming from the outside is only sampled a fraction of the time. Because the chopper acts as a valve between the first and the subsequent pumping stages, the background signal is greatly reduced leading to a very high signal-to-noise ratio. By comparing the signals with the chopper in opened and closed position, the participation to the signal coming from the background can be easily distinguished from the participation from the effluent of the jet. The signal can then be corrected accordingly.
Because CO and N_2 share the same molecular mass, the first sets of measurements will be performed with the COST-jet placed inside of a sealed glass cylinder which will be filled with helium at atmospheric pressure. This prevents the N_2 from ambient air to leak into the mass spectrometer, so that a reference case for the measurements in ambient

air is created. The main parameters that will be changed are the power injected in the plasma and the CO_2 admixture. After that, these measurements will again be attempted in ambient air and compared to the reference case.

Unless explicitly stated, whenever multiple measurements were available, the sets were averaged and the error was computed from the standard deviation. It must be noted however, that an uncertainty of 10 % is commonly understood as the best accuracy one can achieve in any case. For convenience sake, these 10 % uncertainties are not plotted.

3.2.2. Measuring inside a helium atmosphere

As stated before, the COST-Jet will first be placed inside a closed glass cylinder filled with Helium at 1 bar. The main challenge in this environment is preventing the ignition of parasitic discharges inside the jets housing. To solve this problem, the housing was opened up and the electrical components were coated in putty as seen in figure 8. Naturally this

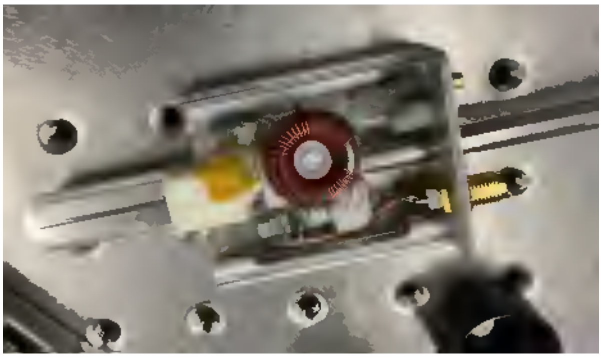

Figure 8: Photo of the “modified” COST-Jet

modification changes the electrical calibration factor and the capacitor will have to be retuned.

Looking at figure 9a, there is a clear difference of the power voltage relation when compared with a regular COST-Jet. While the ignition voltage is very similar, the modified COST-Jet reaches higher powers far faster when compared to the regular one. So the putty significantly alters the circuit. However the reason for that was not investigated. While this makes a direct comparison in relation to the voltage impossible, it should not matter for the measurements themselves, since the behavior of the plasma is dictated by its power and the ignition voltage seems to remain the same. Looking also at the comparison of the COST-Jet with and without housing (figure 9b) it does not seem to make a significant difference whether or not the housing is open or closed as long as the capacitor is tuned accordingly.

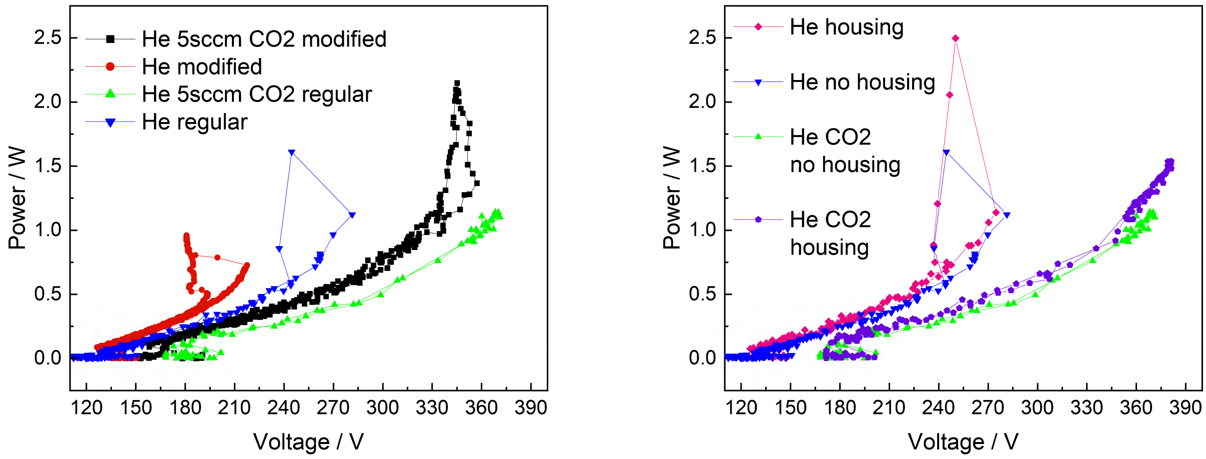

(a) (b)

Figure 9: (a) Power Curves for regular and modified COST-Jet. (b) Power curves for the regular COST-Jet with and without its housing.

Unless explicitly stated, the modified COST-Jet with an open housing was used for all of the measurements

3.2.3. COST-jet placement

To maximize the signal coming from the effluent gas great care must be taken in positioning the COST-Jet. This holds especially true when measuring in ambient air.

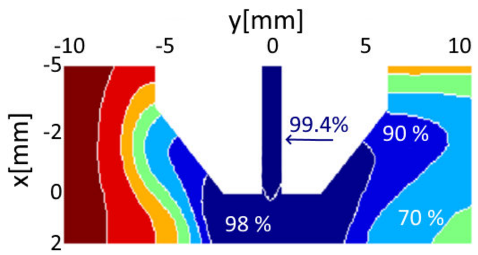

Figure 10: Simulation of gas admixture 2mm in front of a surface. 1.4 slm of He. x is the horizontal position, y the vertical. Adapted from [13]

As figure 10 indicates, the COST-Jet should be as close to the orifice as possible, to minimize the amount of ambient air inside the sampled gas. As discussed in section 2.3.1 the gas is sampled from 200 μm to 500 μm above the orifice. In this case a distance of 3mm to the orifice was achieved.

3.3. OES

The OES setup consists of the jet itself, an optical fiber in the range of the wavelengths of interest and the spectrometer coupled with a CCD-detector (see figure 11a).
The spectrometer (figure 11b) has three different gratings (50, 300 ,1200 grooves/mm) that allow the measurement of three different wavelength ranges with corresponding resolution (e.g. broader range corresponds to lower resolution).
When positioning the optical fiber, it should be aligned with the center of the discharge in between the electrodes.
The OES measurements serve as a quick overview of the species partaking in the plasma chemistry. Since the jet is operated in open air, some degree of back diffusion is unavoidable.

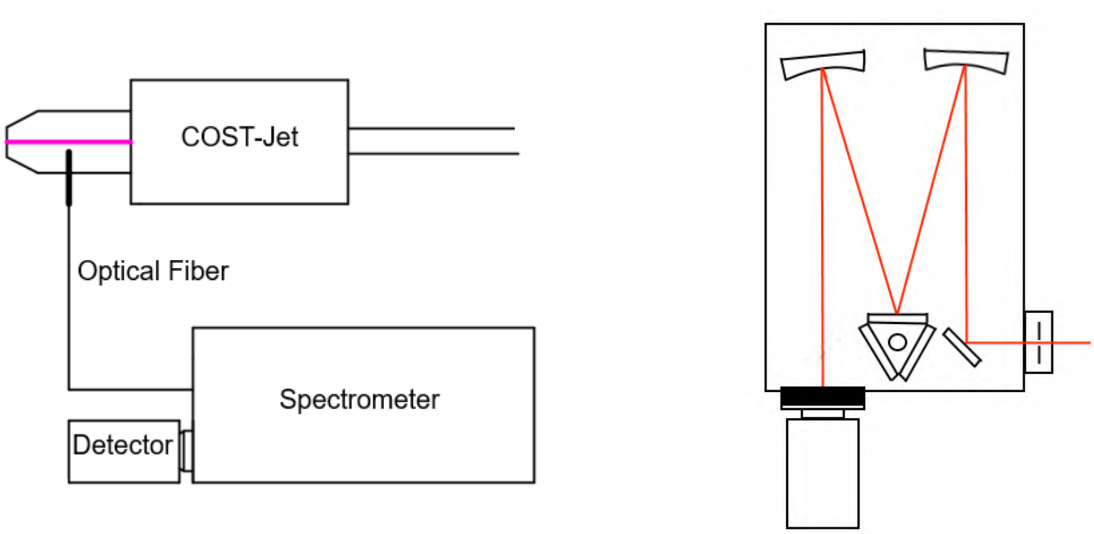

(a) (b)

Figure 11: (a) Sketch of the setup. (b) Sketch of the spectrometer.The red line represents the optical path. Adapted from the HRS-750 manual

4. Results

4.1. OES

4.1.1. Overview

To obtain a quick overview of the species generated in the plasma, the measurements are started with optical emission spectroscopy. The wavelengths chosen for this first test were 260 nm to 380 nm since this range contains the very persistent and easily identifiable 288 nm and 289 nm CO_2^+ bands, the third positive CO system (285-350 nm) and parts of the CO_2^+ Fox Duffenback Barker system (280-450 nm) [14].

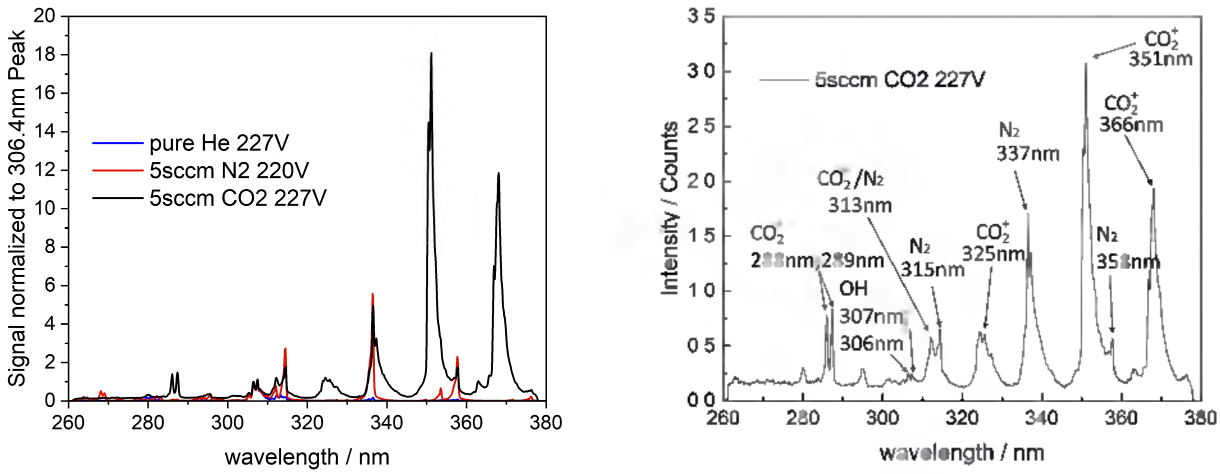

(a) (b)

Figure 12: (a) Spectrum without any admixture, with 4975 ppm of N_2 and with 4975 ppm of CO_2. (b) CO_2 admixed Spectrum with identified bands. The spectra have been calibrated relative to a known reference signal

To simplify Identification, the spectrum of the plasma with 4975 ppm of admixed CO_2 is compared to the spectrum of a pure Helium plasma as well as a plasma with 4975 ppm of admixed N_2 (figure 12a).

Looking at figure 12b, multiple CO_2^+ bands can be identified. Most easily one can identify the 288 nm and 289 nm CO_2^+ bands because of their characteristic appearance. The rest of the CO_2^+ peaks (325 nm, 351 nm, 366 nm) were identified by comparing with the other two spectra and comparing with work by Cepelli et al on optical spectroscopy in a CO_2 ns pulsed discharge [15]. Since these peaks only appear when admixing CO_2 it is evident that they most likely belong to the Fox Duffenback Barker system, albeit the 351 nm

and the 366 nm bands seem irregularly high in terms of intensity. The 313 nm band is an overlap of CO_2 and N_2 bands. Some traces of OH can also be observed at 306 nm and 307 nm. The appearance of OH bands is most likely due to water vapor present either in the gas pipes or in the jet itself.
Since with this setup, the COST-Jet was operated in open air, there is also back diffusion from the open air into the jet. Combined with the fact, that any setup is bound to have some impurities, it is not surprising that N_2 bandheads can be observed.
One thing that should be pointed out, is that there are no visible CO band structures. In part this is due to overlap of the nitrogen peaks, more importantly however, it suggests that there is little to no CO produced in the discharge. Comparing with the paper by Celeppi [15], there should be visible CO bands in the 285 nm to 350 nm range. Assuming that little to no CO is produced, these bands likely overlap with noise or other bands.

4.1.2. Voltage variation

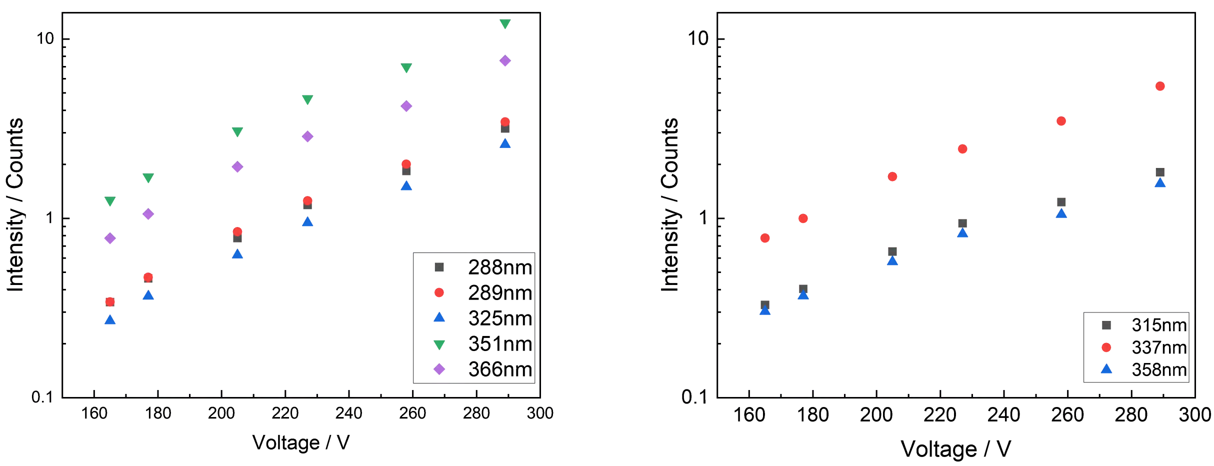

(a) (b)

Figure 13: Bandheads as function of voltage at 4975 ppm of CO_2 admixture (a) CO_2 (b) N_2

When increasing the voltage (figure 13) an increase in the intensity of all bandheads is observed. In agreement with the fact that an increase in voltage causes an increase in electron density rather than temperature, this increase in intensity is similar for all species.

4.1.3. Admixture variation

It must be noted, that the power was not adjusted after admixing more CO_2, because at that point, the power measurements were not properly implemented. Because CO_2 is highly electronegative, it draws electrons thus decreasing the electron temperature, since the energy of the electrons is dispersed in the excitation of the vibrational and rotational states of CO_2. This leads to the loss of power inside the plasma. Consequently the intensity of the whole spectrum decreases. Because most of the gas in the discharge is helium, the helium line can be used to normalize the intensities of different bands according to the power lost by admixing more CO_2. This allows the examination of the relative intensities.

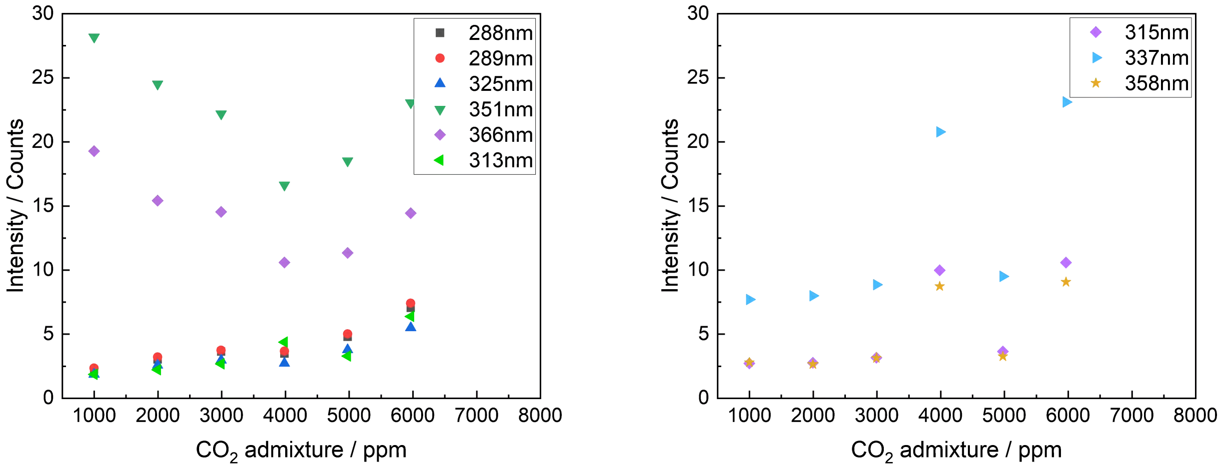

(a) (b)

Figure 14: Bandheads as function of admixture for (a) CO_2 at 227 V (b) N_2 at 220 V

Starting with the CO_2^+ bands for the higher energy part of the spectrum (up until 325 nm) there is a clear increase in intensity corresponding to the plasma power being dispersed in the excitation of CO_2, while for the rest of the band structure there seem to be a minimum at around 4000 ppm (figure 14a). It can be speculated that the energy levels associated with the 366 nm and 351 nm bands are close to some excited state of helium that is energetically favored or it may hint to the fact, that these two bands belong to another system entirely, considering that the other CO_2 bands shown here behave differently. However, this could not be investigated in this study.
The evolution of the N_2 bandheads seems arbitrary. That could be the consequence of back diffusion into the jet, causing this serrated pattern in the bandheads. The same

pattern can be seen in the 313 nm CO_2 band, since it overlaps with a low intensity N_2 band. Another possibility might be that the nitrogen measured is an impurity introduced by earlier measurements, but seeing as the system was flushed beforehand and that the measurements done with an intentional N_2 admixture were conducted last, it is unlikely. When comparing both the CO_2 and the N_2, the minima of the CO_2 bandheads are exactly where the N_2 ones have a maximum. However, a more thorough investigation would be necessary to discern the behavior of the N_2 bandheads as anything but a measuring error. Because the intensities of the OH bands are very low when compared to the other bands, they are excluded from investigation.

4.2. Mass spectrometry in helium atmosphere

Considering that CO and N_2 have the same molecular mass (28 amu), it will be problematic to measure CO in open air, since the N_2 signal from the ambient air will overlap with the CO signal from the effluent of the jet.
To circumvent this problem the measurements in helium atmosphere will serve to check if it is possible to measure CO through the loss of CO_2, since the only loss channel should be its dissociation. Going forward, the measurements done with a turned off discharge will be referred to as background measurements. It is important to note that CO_2 can also be dissociated by the ionizer inside the mass spectrometer (see section 2.3.6). While this has little effect on the measurements of CO_2, it will overestimate the amount of CO measured because of the appearance of dissociatively ionized CO. Necessarily an energy of 18 eV was chosen, since it is between the appearance threshold by dissociative ionization (19 eV, [10]) and the ionization energy for CO (14 eV, [16]). Similarly for the O measurements, an energy of 16 eV was chosen, because it is in between the ionization energy 13.6 eV [17] and the dissociative ionization threshold 17.3 eV [18]. The same method has been used by Willems [10].
To obtain the density of CO, O and O_2, the measurements taken with the discharge turned on are then subtracted by the background. For the CO_2 loss, the background was subtracted by the measurement with the ignited plasma.

4.2.1. CO_2 as an indirect way to measure CO

Beginning with the CO_2 (figure 15a). The behavior is generally as one would expect, with rising power, there is a decrease in CO_2, because more CO_2 is dissociated. However this decrease is very small. Also, as evident from the comparison of the two measurements in figure 15a and figure 30 (Appendix A), the fluctuations in the densities between sets of measurements is greater than their decrease, suggesting that this indirect way of measuring CO might not be possible. This is especially evident when looking at the CO_2 loss (figure 15b). Even the fluctuation in the background acquired on the same day are greater than the increase in CO_2 loss.

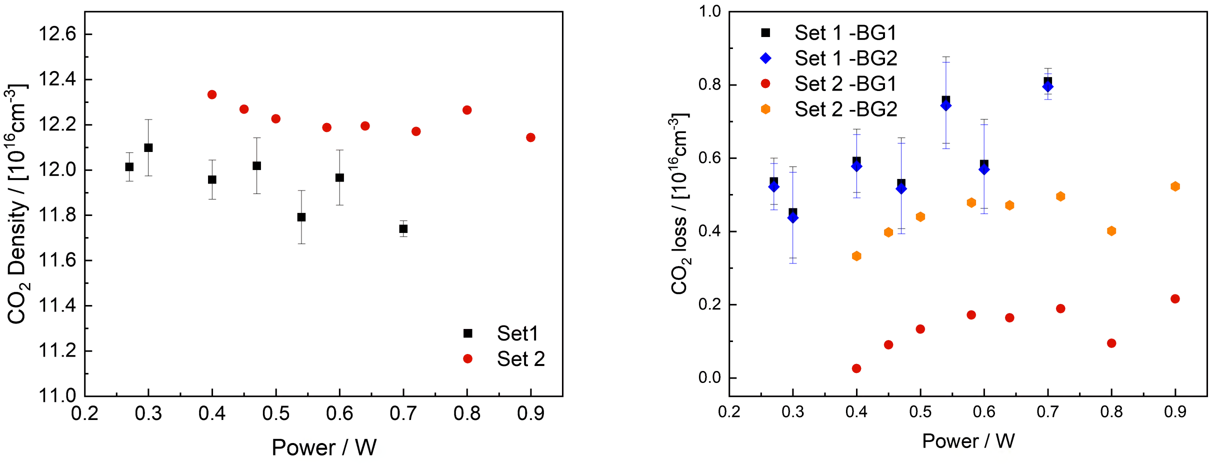

(a) (b)

Figure 15: (a) CO_2 densities as function of plasma power at a CO_2 admixture of 4975 ppm. (b) CO_2 loss as function of plasma power at 4975 ppm. BG1 refers to the background taken prior to measurement, BG2 to the one taken after.

4.2.2. Evolution of the CO densities

Looking at the CO evolution (figure 16), with rising power there is a rise in the amount of CO measured, according to the increase in the dissociation of CO_2. The density evolves from $0.04{\cdot}10^{16}\,cm^{-3}$ to $0.11{\cdot}10^{16}\,cm^{-3}$ and in this case the difference in whatever background is chosen for subtraction is minimal and within a 10 % margin, so in light of the achievable accuracy, the CO background seems to be stable.

Comparing now the measured CO densities with the CO_2 loss, the difference in density is evident, with the CO densities being below the loss in density of CO_2. The lowest

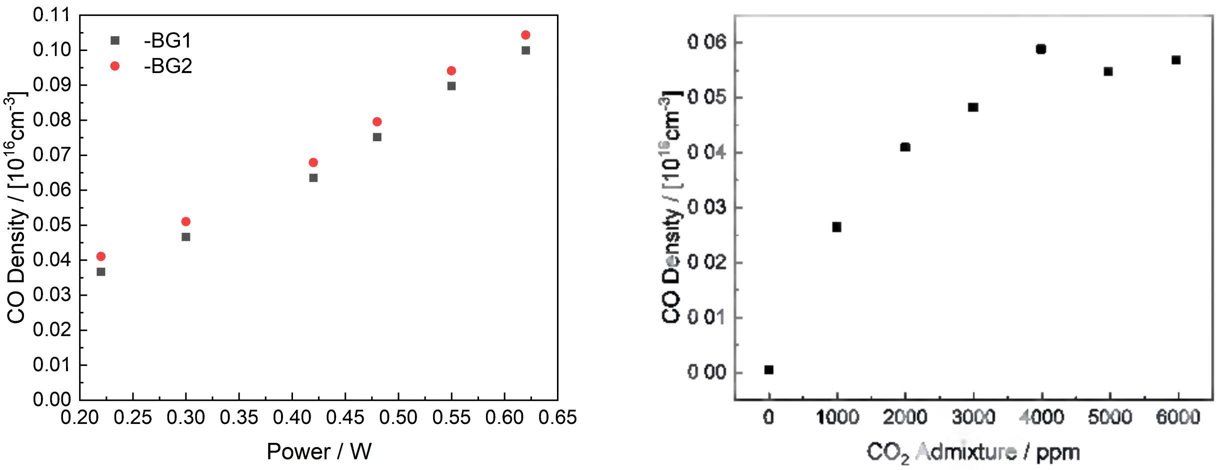

(a) (b)

Figure 16: (a) CO density as function of plasma power at a CO_2 admixture of 4975 ppm. BG1 refers to the background taken prior to measurement, BG2 to the one taken after. (b) CO density as function of admixture at 0.3 W for 6000 ppm.

calculated CO_2 loss is twice as high in density as the measured CO. When admixing more CO_2, the measured CO density increases at first and plateaus at 3000 ppm, resembling a saturation curve. This is due to the power not being corrected after increasing the admixture. This was again because the power measurement did not work yet (the measurements here were done as a function of the voltage, which was later converted to the power). Nevertheless a maximum at 4000 ppm was observed.

To calculate the conversion rate, the input of the mass flow controller (MFC) serves as the initial amount of CO_2, since the measured CO_2 densities are unreliable :

$$R = \frac{[CO]_{plasmaOn}}{[CO_2]_{MFCinput}} \tag{14}$$

In this case a conversion rate of between 0.3 % and 1 % was observed. Comparing this result with the conversion rate calculated by Willems at 1.65 % [10], both remain within the same range of below two percent. With a setup designed to maximize conversion [19], Stewig et al were able to reach conversion rates surpassing 50 % when operating their plasma source at a high power [20]. The low conversion rate of the COST-jet might be due to the residence time of the CO_2 being too low. However this was not investigated as part of this study, since in this case a low conversion is not concerning, seeing as the goal is to produce small amounts of CO.

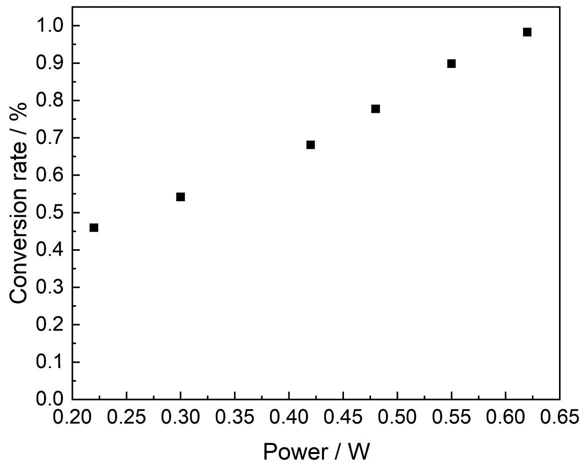

Figure 17: conversion rate as function of power at a CO_2 admixture of 4975 ppm.

4.2.3. Pseudo-stoichiometry

Accounting for the fact that the CO_2 losses do not add up with the measured density of CO, any attempt at checking the carbon balance of this system would be in vain.
Instead using equation 3 and 2, it is possible to check for self-consistency because CO, O and O_2 are the only possible products of CO_2 dissociation (technically also O_3 but its density is negligibly small, see figure 32, Appendix A). So by adding up the densities of O and O_2 according to their stoichiometric ratio and comparing that to the CO density, it is possible to check for self consistency.
First looking at the evolution of oxygen by itself (figure 18a) there is a seemingly linear correlation between the power and the density of both atomic and molecular oxygen. In agreement with the assumption that the radical oxygen is highly reactive and quickly recombines, the O_2 far outweighs the O in terms of density. While the molecular oxygen reaches densities up to $0.06{\cdot}10^{16}\,\mathrm{cm}^{-3}$, its atomic counterpart only varies from 0.01 to $0.02{\cdot}10^{16}\,\mathrm{cm}^{-3}$. Because the backgrounds were nearly identical for both O and O_2 , only the computed densities using the backgrounds taken after the measurements are shown.
When examining this pseudo-stoichiometry, the measured density of the CO is compared with twice the measured density of molecular oxygen plus the measured density of the atomic oxygen. Ideally these densities should be exactly the same.
In this case (figure 18b), the densities are in very good agreement, indicating that the

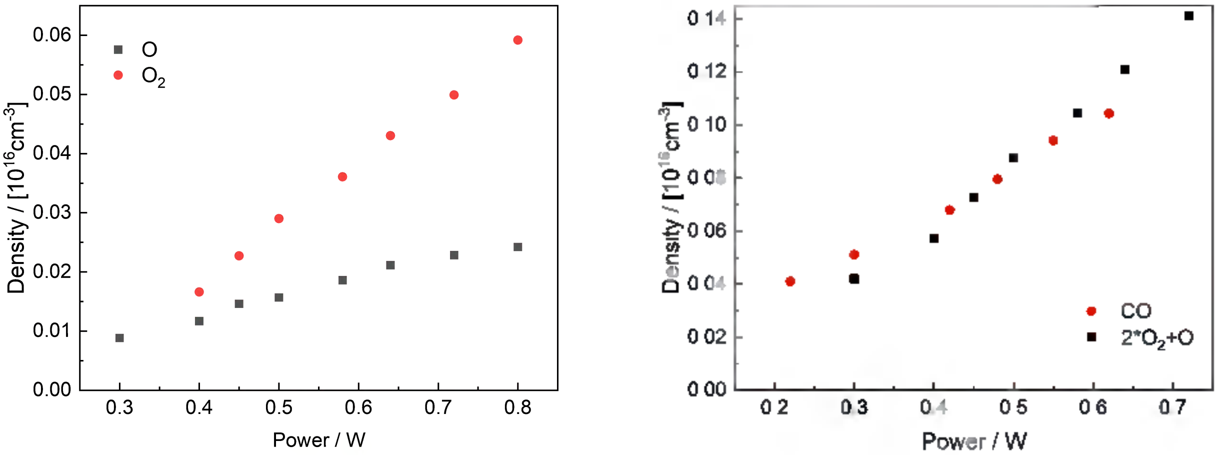

(a) (b)

Figure 18: (a) O2 and O densities as function of power at a CO_2 admixture of 4975 ppm. (b) Pseudo stoichiometry as function of the power at a CO_2 admixture of 4975 ppm.

measurements are self consistent.

Because the backgrounds for all species except CO_2 are stable, the backgrounds taken after the measurements with the discharge turned on will be used during the rest of this study .

4.3. Mass spectrometry in ambient air

Now that the reference case with the helium atmosphere has been investigated, the main trials in ambient air can begin.

The top of the glass cylinder confining the helium atmosphere is removed while the cylinder itself is kept in order to reduce the effects of turbulence from ambient air. With the COST-Jet outside the helium atmosphere, a wider range of power can be applied as the ignition of parasitic discharges is no concern in open air. Hence the range of power investigated spans from slightly above ignition to the point where the jet begins to constrict.

The first aspect worth investigating is the behavior of the CO_2 in ambient air to see if the same fluctuating behavior can be observed as with the helium atmosphere.

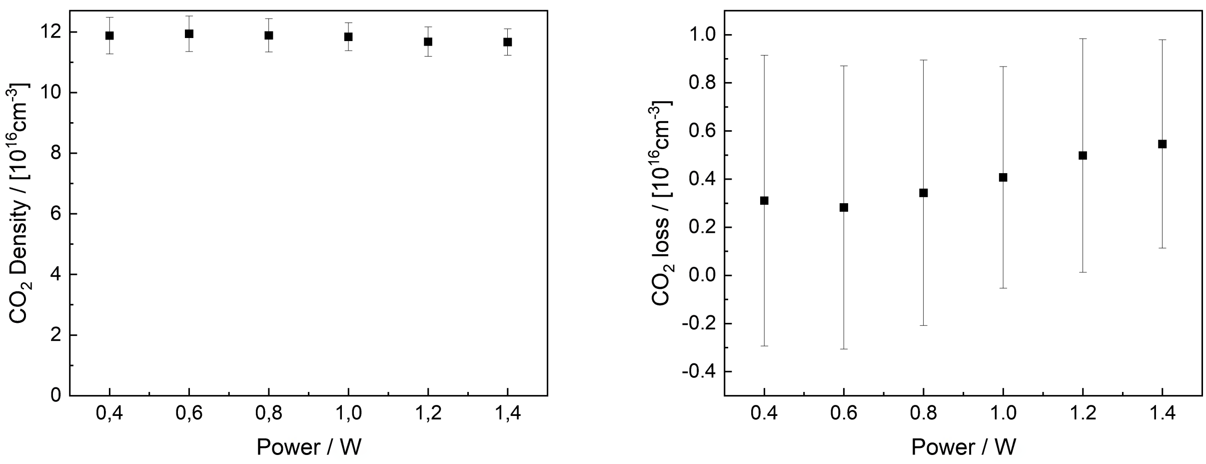

(a) (b)

Figure 19: (a) CO_2 density (b) CO_2 loss as function of the power at a CO_2 admixture of 4975 ppm averaged over the sets done in ambient air.

4.3.1. Examination of CO_2 in ambient air

Averaging over the measurements conducted in ambient air (figure 19), it is evident by the large uncertainties of both the CO_2 density and the CO_2 loss, that the behavior of the CO_2 remains unchanged and considering the order of magnitude of the CO densities (10^{14} to 10^{15}), these uncertainties are far too large to get meaningful results.

Because CO_2 is not suitable to indirectly measure CO, another method has to be used to obtain the CO densities.

4.3.2. CO measurement using TIMS

Using TIMS, the participation of N_2 to the CO signal can be isolated, since the ionization energy of N_2 at around 15.6 eV is higher than that of CO at around 14 eV ([21], [16]) The problem however is that the ionization energy output of the ionizer is slightly shifted. To calibrate the energy output, a scan over the applied voltage of the ionizer, responsible for accelerating electrons to the desired energy, is conducted. With the discharge turned off (figure 20b), no signal can be detected up to 18 V. Increasing the voltage further leads to a significant increase in signal in accordance to the direct ionization of N_2. When turning on the discharge (figure 20a), there is already a less pronounced increase of the signal starting at 16.4 V, corresponding to the ionization of CO. At 17.9 V the signal increases more rapidly, as N_2 is also ionized. By linearly fitting a line to the

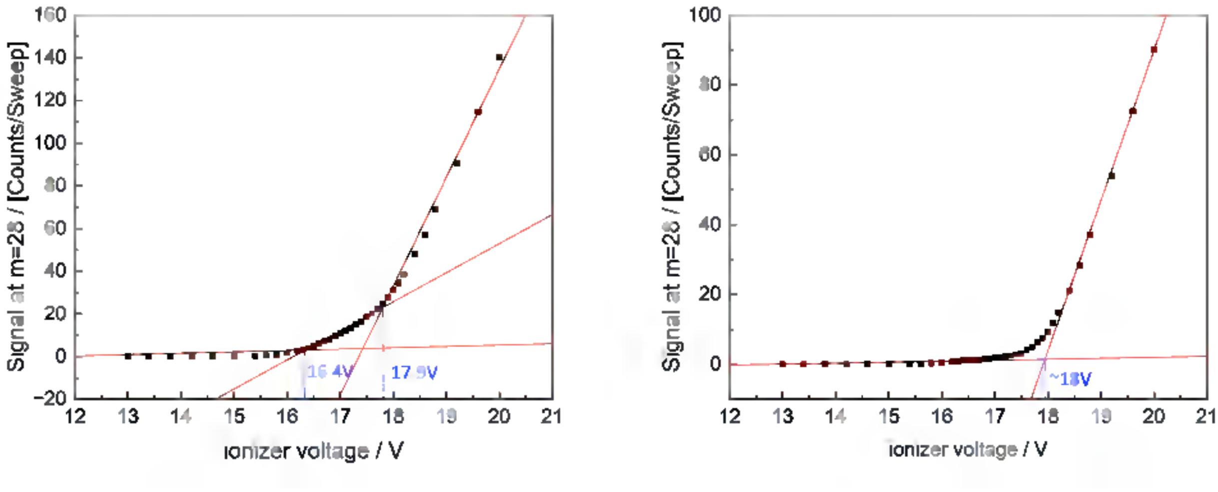

(a) (b)

Figure 20: Scan of the applied voltage of the ionizer at mass m=28 amu with a CO_2 admixture of 4975 ppm in ambient air (a) with turned on discharge (b) with turned off discharge

respective ranges of the different slopes, the intersections between the different lines can be computed thus revealing the corresponding voltage to the respective ionization energy. Here the shift from the input voltage on the ionizer to the actual output energy is around 2.3 to 2.4. (figure 20a, figure 20b). In this case, the 2.4 shift was chosen since a possible overestimation of the shift by 0.1 does not matter for minimizing the participation of N_2 to the signal.

The actual energy that was chosen for the ionizer was 15 eV because the cross section at 15 eV is already known (see Appendix B) and it is below the threshold of ionization for N_2.

As long as this change in ionization energy is accounted for during data treatment, it should not have an effect on the outcome of the measurement other than increasing the necessary acquisition time.

One of the most important aspects left to investigate is the influence of the ambient air on the measurements.

The evolution of the CO density as function of the power (figure 21a) suggests a linear behavior in the lower power parts ranging from 0.4 W to 0.8 W, which flattens at higher powers. This implies that the curve tends to some saturation density, albeit the jet begins to arc above 1.4 W. When comparing these results with the ones found in the helium atmosphere, the densities are still in good agreement, even though the results obtained

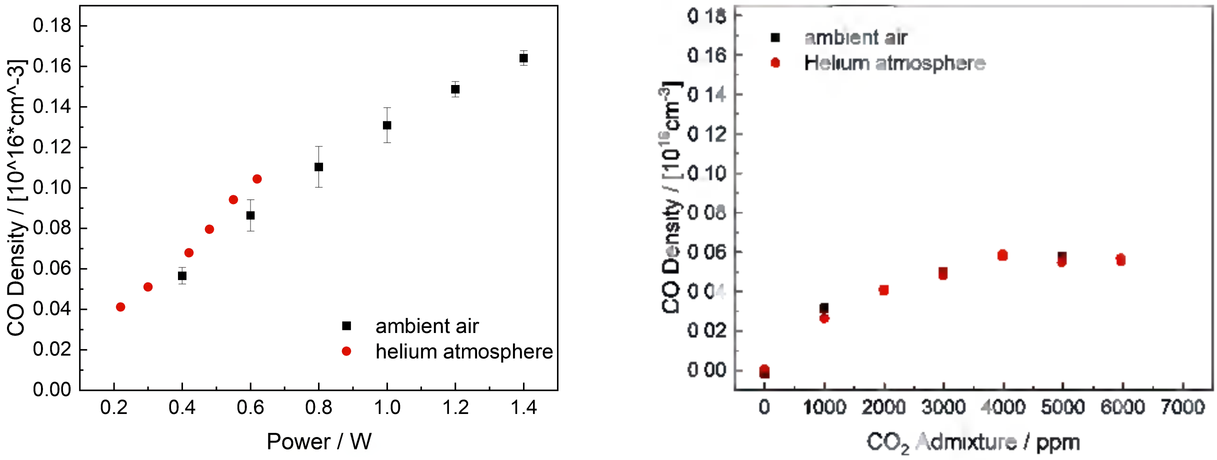

(a) (b)

Figure 21: (a) Evolution of the CO density as function of the power at a CO_2 admixture of 4975 ppm compared to previous measurements. (b) Evolution of the CO density as function of the admixture, at 0.3 W for 6000 ppm compared to previous results.

in helium are slightly above what was found in ambient air. This small shift might be explained by the fact, that for the measurements in helium, the measured voltages had to be converted to powers in post treatment and since the setup with the helium atmosphere was different in terms of electrical calibration factor (due to cable length and additional connectors), the voltages used when converting might have been slightly different than the actual voltages that were applied during the helium atmosphere measurements.
For the variation of the admixture (figure 21b), both results are basically identical. This is reassuring regarding the effects of the ambient air on the measurements, suggesting that the error that is introduced through the ambient air is very small, at least when measuring CO. It also demonstrates, that the participation of N_2 to the CO signal can be eliminated using TIMS.

Additionally the evolution of the CO density as a function of CO_2 admixture is investigated at a power of 1.3 W (figure 22). For one of these measurements, the power was kept at 1.3 W for all admixtures. Comparing first of all the measurements taken at 1.3 W (figure 22) with the measurements at 0.3 W (figure 21b). Whereas previous measurements saturated at around $0.6 \cdot 10^{16}\,cm^{-3}$ at 0.3 W, with a power of 1.3 W the saturation value now lies at about just below $0.16 \cdot 10^{16}\,cm^{-3}$, so just about two and a half times of what was recorded with a lower power.

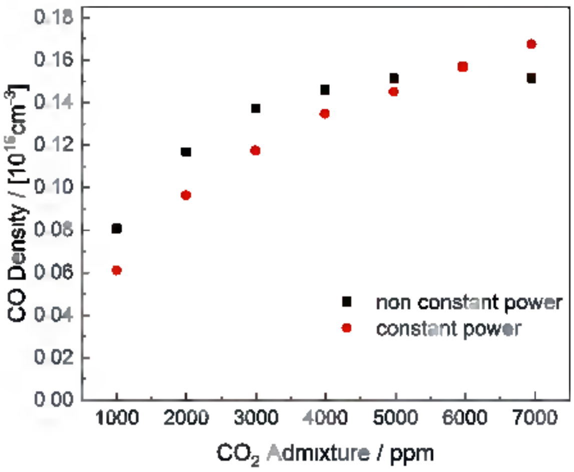

Figure 22: Evolution of the CO density as function of the admixture at 1.3 W for 6000 ppm and at a constant 1.3 W for all admixtures.

Comparing this result with the measurement done at a steady power of 1.3 W for all admixtures (figure 22), there are some minor differences. Starting with the part leading up to 6000 ppm. With a constant power, the densities are all below the ones with non constant power, since when lowering the admixture from 6000 ppm, the plasma power increases because there is less CO_2 inhibiting the discharge. This effect becomes more severe the smaller the admixture. When approaching 6000 ppm both cases line up perfectly as expected, since 6000 ppm is the reference point. Surpassing that point the steady case displays a higher density. It is noteworthy that at steady power, the evolution of the CO density flattens, implying that it might also reach a saturation value or a maximum at high CO_2 admixture.

Looking at the conversion rates (figure 23) and first comparing again the results from ambient air with the ones obtained in a helium atmosphere, although there is no direct overlap between the measurements, the results are only a few per mille apart and thus in good agreement, just as the absolute densities were in figure 21a. The conversion rate seems to decay with increased admixture, starting from about 3.2 % dropping to about 1 %.The conversion rate for the case with constant power compared to the non constant case, behaves exactly as the absolute densities in figure 22.

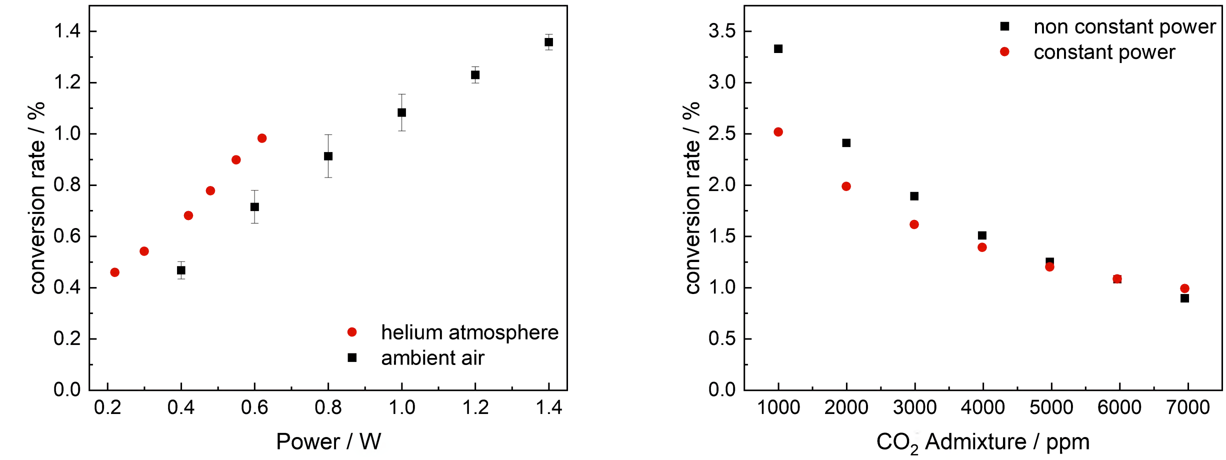

(a) (b)

Figure 23: (a) Conversion rate of CO from CO_2 as a function of power at a CO_2 admixture of 4975 ppm. For the initial CO_2, the input on the MFC was taken. (b) conversion rate of CO from CO_2 as function of admixture at 1.3 W.

4.3.3. Pseudo-stoichiometry in ambient air

In order to check the pseudo-stoichiometry again, both atomic and molecular oxygen must first be investigated.

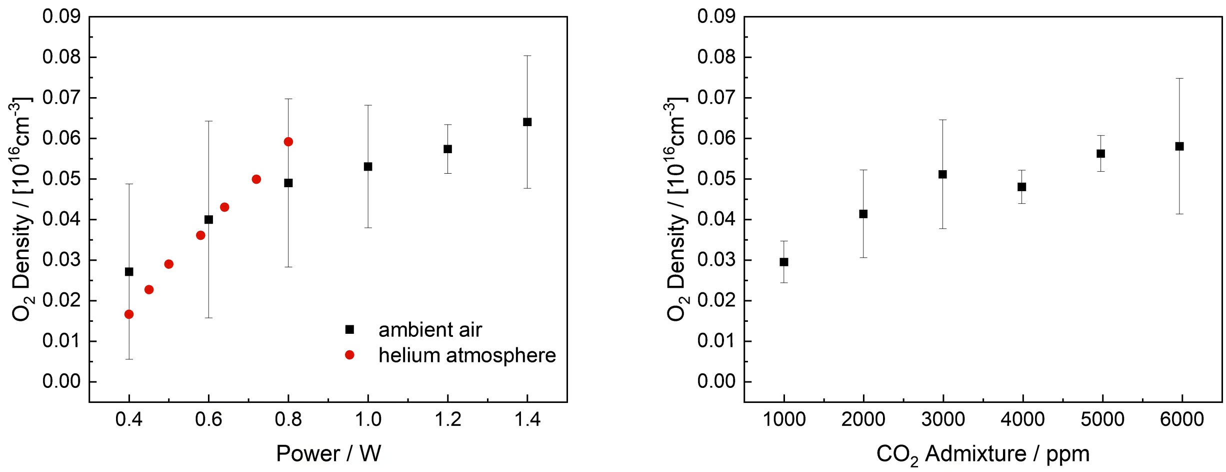

(a) (b)

Figure 24: (a) O_2 density as function of the power at a CO_2 admixture of 4975 ppm.(b) O_2 density in relation to the admixture for 1.4 W at 6000 ppm.

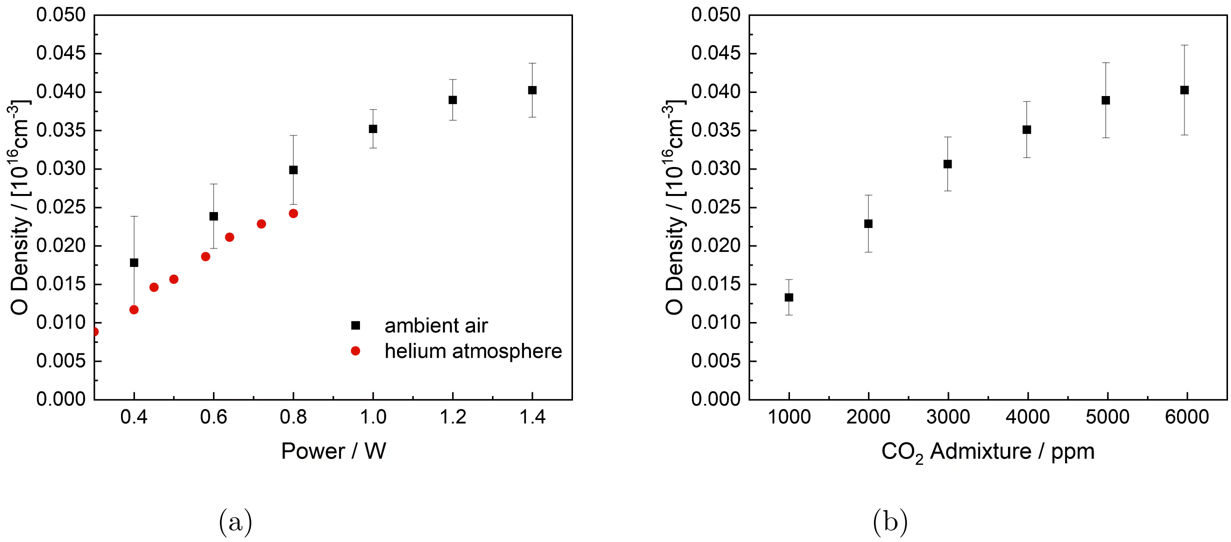

Figure 25: (a) O density in relation to the power at a CO_2 admixture of 4975 ppm. (b) O density in relation to the admixture for 1.4 W at 6000 ppm.

The large uncertainties observed in the O_2 measurements (figure 24) may hint to the fact, that the measurements are perturbed due to oxygen from the ambient air mixing in with oxygen from the effluent. Nevertheless the general tendency of the results is consistent, especially considering that the densities of the measured species are really low (in the 10^{14} range). With rising power the O_2 density increases, ranging from $0.005{\cdot}10^{16}\,\mathrm{cm}^{-3}$ to $0{,}08{\cdot}10^{16}\,\mathrm{cm}^{-3}$. Comparing with the result from the helium atmosphere, there is a clear overlap between both measurements. However the rate at which the densities increase differs in both cases. In the helium atmosphere, the increase is much steeper, whereas in ambient air, the O_2 gain is much less pronounced. The same behavior is shown in the admixture variation. Only a slight increase from $0.03{\cdot}10^{16}\,\mathrm{cm}^{-3}$ to $0.055{\cdot}10^{16}\,\mathrm{cm}^{-3}$ can be seen and even at lower admixtures, the O_2 density is still comparatively high. Nevertheless these results fit nicely with the ones obtained in helium, although they may highlight the fact that even a small leak can cause a noticeable change in measurements of species with a low density that are also present in ambient air.

For the measurements of atomic oxygen (figure 25), this should not be a problem, because there is no atomic oxygen in ambient air. Hence the results obtained from the different sets of measurements are also more similar leading to smaller error bars. Looking at the power evolution (figure 26a), similar densities were measured in ambient air and in the helium atmosphere. Further increasing the voltage leads to an increased O density of $0.04{\cdot}10^{16}\,\mathrm{cm}^{-3}$.

Varying the admixture of CO_2 leads to a saturation curve similar with what was found for CO. The densities that are reached also fit in with the densities reached when varying the power.

As seen in figure 26, despite the large uncertainties, the densities match up. Thus it is safe to assume that the measurements are self consistent, seeing as the pseudo-stoichiometry is fulfilled and that the ambient air measurements are all in good agreement with the reference case in the helium atmosphere. This leads to the conclusion that attempting measurements in ambient air has no major effect on the results, as suggested by the simulation done by Kelly et al [13] that was shown in figure 10, predicting that the area close to the nozzle is mostly made up of the effluent of the jet, when in close distance to a surface.

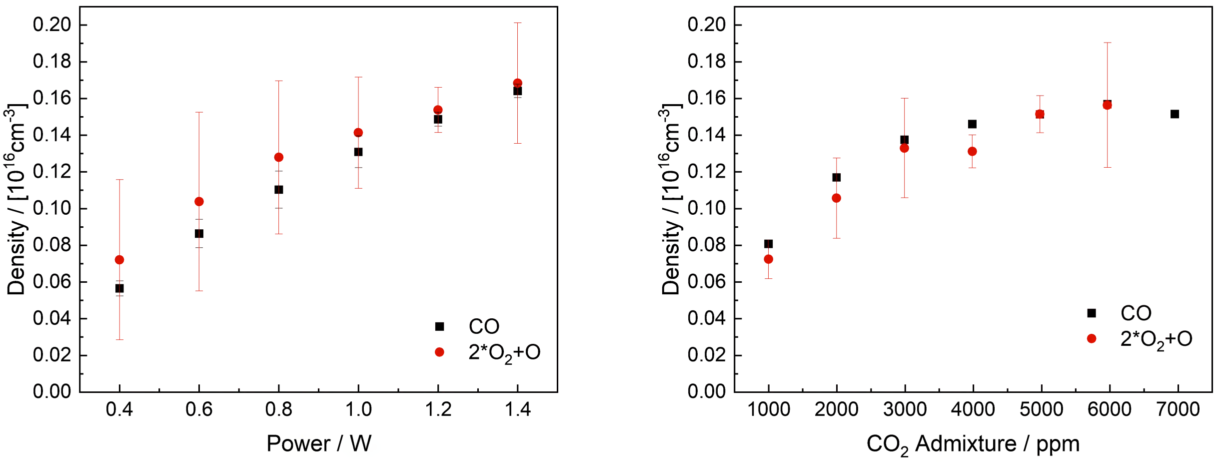

(a) (b)

Figure 26: (a) Pseudo stoichiometry as a function of the power at a CO_2 admixture of 4975 ppm. (b) Pseudo stoichiometry as a function of admixture at 1.3 W for CO and 1.4 W for O and O_2. Error calculated through propagation of uncertainty.

4.4. Comparison to CO measurements by gas analysis

During a research stay in Orleans, additional data for the COST-Jet could be obtained. The measurements there were done using an unmodified COST-jet with closed housing. The diagnostic used was a gas analyzer based on infrared absorption. The plasma power in this case was limited by the output of the power supply. In order to acquire the

CO concentration from the effluent, the measured CO must be corrected according to the discrepancy in the concentration of O_2 measured by the gas analyzer and the concentration of O_2 in ambient air.

$$[CO]_{plasma} = \frac{[CO]_m - [CO]_{air}}{[O_2]_{air} - [O_2]_m} * [O_2]_{air} \approx \frac{[CO]_m}{[O_2]_{air} - [O_2]_m} * [O_2]_{air} \tag{15}$$

The concentrations with the subordinate "m" refer to the ones measured by the gas analyzer, the ones with subordinate "air" to the ones present in ambient air. By multiplying the CO concentration with the ratio of the Avogadro number and the molar volume of an ideal gas, the absolute densities can be obtained. The uncertainties were calculated from the O_2 percentage of the sampled gas inside the gas analyzer.

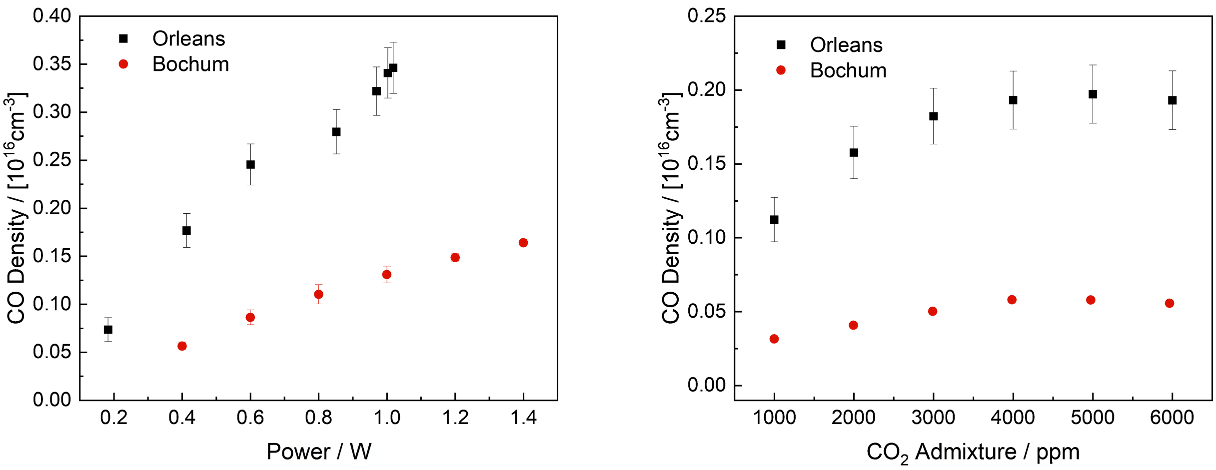

(a) (b)

Figure 27: Evolution of the CO density as function of (a) the power for a CO_2 admixture of 4975 ppm. (b) the CO_2 admixture. The Orleans measurements were conducted at 0.4 W, the Bochum measurements at 0.4 W.

Comparing the results from Bochum with the ones from Orleans, the latter show higher absolute densities. When varying the power (figure 27a), the densities measured by the gas analyzer increasing far more rapidly, reaching a maximum value of $0.35 \cdot 10^{16}\,\mathrm{cm}^{-3}$ for 1 W. The densities measured in Orleans are about 3 times higher when compared to the densities measured in Bochum.
Similarly the absolute densities measured as function of of the CO_2 admixture differ by a factor 3 (figure 27b). It should be noticed that the injected power differs slightly for both diagnostics due to practical reasons, nevertheless this does not affect the measurements

enough to obtain a factor of 3. Considering that the measurements are still consistent within the same order of magnitude, despite the fact that different diagnostics were used, the results are in good agreement.

Nevertheless since the factor 3 is prevalent, it is worth investigating the ratio between the mass spectrometry and the gas analyzer results to see if this factor is stable.

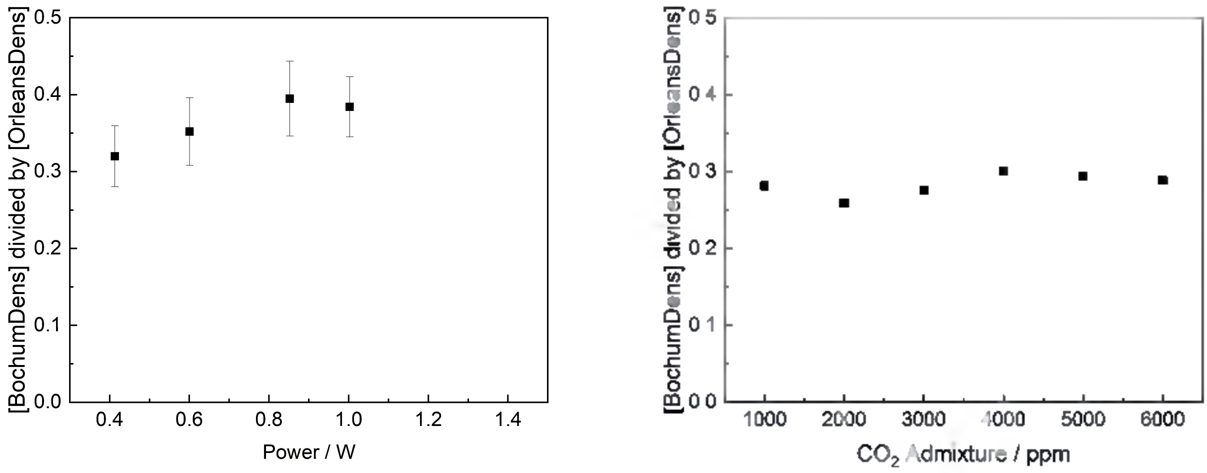

(a) (b)

Figure 28: Ratio of the absolute densities measured in Orleans over the absolute densities measured in Bochum (a) as a function of power (b) as a function of admixture

Both when changing the power and the admixture (figure 28), the factor between the two measurements appears constant, implying there is a correction factor to apply.
The fact that the only discrepancy between measurements from both diagnostics seems to be a constant factor means, that both diagnostics deliver comparable results.

5. Conclusion and outlook

In the wake of the investigation of atmospheric pressure plasma for biological and medical application and considering the promising effects of CO in medical treatment, this study aims to characterize the CO production of an atmospheric pressure plasma in ambient air, by measuring the absolute densities of the species produced by the dissociation of CO_2.

The COST-jet was used as a plasma source because it is has been extensively studied in the past and it is suitable for medical applications. Mass spectrometry was chosen as the main diagnostic since it allows the measurement of low density species.

A first overview of the species was obtained through optical emission spectroscopy, already implying a low production of CO on account of the lack of visible CO bands.

The first trials of the mass spectrometry measurements were done inside a helium atmosphere to create a reference case for the measurements in ambient air. The results from the helium atmosphere have shown that the measurement of the CO_2 loss is not suitable as an indirect way to measure CO, due to the fluctuations of the CO_2 densities being greater than the densities of CO.

To investigate the self consistency of the CO, O and O_2 measurements, the densities of said species were compared according to the stoichiometry of the chemical equation for the dissociation of CO_2, proving that the measurements are indeed self consistent.

The first assumption according to the OES measurement that there is little to no CO being produced, was confirmed by the low conversion rate between 0.3 % to 1 %, similar to the 1.65 % obtained by Willems with a similar setup and similar parameters [10].

When continuing the mass spectrometry measurements in ambient air, threshold ionization mass spectrometry was used to bypass the overlap of the N_2 and CO signals, making the measurement of CO in ambient air possible.

Through comparison with the reference case created by the measurements inside the helium atmosphere, it was demonstrated that there is no major difference in the results when measuring in ambient air. It must be ensured however, that the COST-Jet is properly positioned close to the orifice, because even small leaks can cause a noticeable difference in measurements of low density species that are also present in ambient air.

The ambient air measurements were proven to be self consistent, applying the same method used in the helium atmosphere. When comparing the results obtained by mass spectrometry with the results obtained by using a gas analyzer, the results have shown to be in good agreement within the same order of magnitude, displaying a consistent

factor of three when comparing the absolute densities obtained by the two diagnostics. To make future comparisons with the setup of the gas analyzer possible, this factor three difference must be investigated.
Going forward it will also be interesting to examine the reason behind the CO_2 measurements fluctuation, since it should not matter for the mass spectrometer whether or not the CO density is measured directly, or through CO_2, given its high accuracy.
Regarding the COST-jet it will also be interesting to examine the absolute densities of the species as a function of the distance to the orifice, since when put in the context of medical application, especially regarding local treatment, a short distance to the target area cannot always be ensured.

Fazit und Ausblick

Im Zuge der Untersuchung von atmosphärendruck Plasmen mit Hinblick auf dessen Nutzung in der Medizin und aufgrund der vielversprechenden Effekte von CO in der medizinischen Behandlung, wurde in dieser Arbeit die CO Produktion in einem atmosphärendruck Plasma in der Umgebungsluft, durch die Messung der absoluten Dichten der bei der Dissoziation von CO_2 auftretenden Produkte, charakterisiert.
Da der COST-Jet in der Vergangenheit bereits ausgiebig erforscht wurde und er geeignet für die Nutzung in der Medizin ist, dient er hier als Plasmaquelle.
Das Hauptdiagnostikverfahren ist in diesem Fall die Massenspektrometrie, welche die Messung von Spezies mit niedrigen Dichten ermöglicht.
Durch optische Emissionspektroskopie wurde ein erster Überblick über die verschiedenen Spezies geschaffen, der bereits darauf hindeutete, dass nur geringe Mengen an CO produziert werden.
Die ersten Messreihen in der Massenspektrometrie wurden innerhalb einer Helium Atmosphäre durchgeführt, um später einen Vergleich mit den Messungen in der Umgebungsluft zu ermöglichen. Die Messungen in der Helium Atmosphäre zeigten, dass die indirekte Messung von CO über den Verlust an CO_2, aufgrund hoher Ungenauigkeit der CO_2 Messungen relativ zur gemessenen CO Dichte, nicht möglich ist.
Um die Selbstkonsistenz der CO, O und O_2 Dichten zu überprüfen, wurden die absoluten Dichten eben genannter Spezies im Bezug auf ihr stoichiometrisches Verhältnis zueinander verglichen. Hierbei wurde die Selbstkonsistenz der Messungen bewiesen.
Die erste Annahme aus den OES Messungen, dass nur sehr wenig CO produziert würde, konnte durch die geringe Konversionsrate von nur 0.3 % bis 1 % bestätigt werden. Eine ähnliche Konversionsrate von 1.65 % konnte bereits durch Willems an einem ähnlichen Setup mit ähnlichen Parametern gemessen werden [10]
Bei Durchführung der Messungen in der Umgebungsluft konnte gezeigt werden, dass die Überschneidung der gemessenen Signale von N_2 und CO durch TIMS umgangen werden kann, um so die Messung von CO in der Umgebungsluft zu ermöglichen.
Der Vergleich hat gezeigt, dass es keinen bedeutsamen Unterschied in den Ergebnissen aus der Helium Atmosphäre und denen aus der Umgebungsluft gibt. Es konnte ebenfalls durch den Vergleich der stoichiometrischen Verhältnisse gezeigt werden, dass die Messungen in der Umgebungsluft selbstkonsistent sind.
Die CO Dichten die mittels Massenspektrometrie gemessen wurden, zeigten eine gute Übereinstimmnug, innerhalb der selben Größenordnung, wie die durch einen Gas Analysator

gemessenen CO Dichten. Hierbei unterschieden sich gemessenen CO Dichten beider Diagnostiken lediglich um einen konstanten Faktor drei.
Um zukünftige Vergleiche beider Diagnostiken zu ermöglichen, sollte dieser Faktor untersucht werden.
Außerdem gilt es, den Grund für die bei der CO_2 Messung beobachtete große Ungenauigkeit, relativ zur CO Dichte, auszumachen.
Bezüglich des COST-Jets ist es interessant, die absoluten Dichten der Spezies abhängig von der Entfernung zur Massenspektrometeröffnung zu messen, da im Hinblick auf die Nutzung auf lokale medizinische Behandlung kein fester Abstand zum Zielgebiet der Behandlung gewährleistet werden kann.

A. Additional Graphs

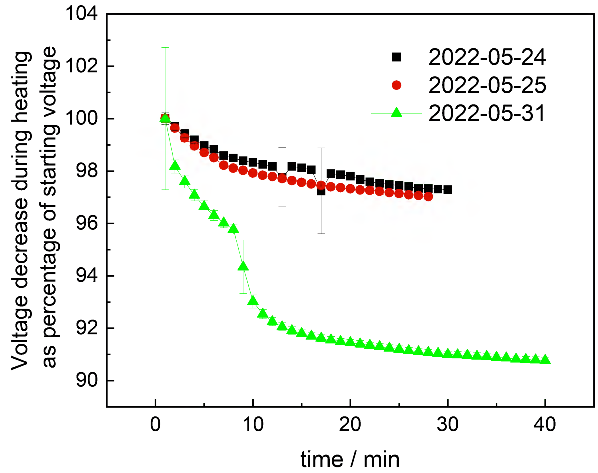

Figure 29: Voltage drop from initial voltage in percent as function of time measured on different days. The most drastic change occurs within the first 15 min.

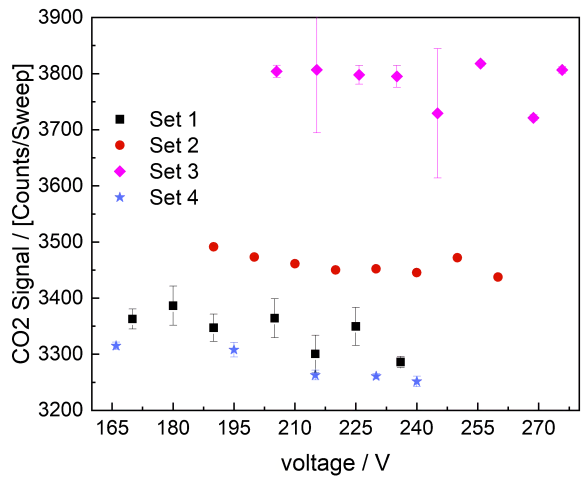

Figure 30: CO_2 density measurements on different days at a CO_2 admixture of 4975 ppm, without post treatment in helium atmosphere

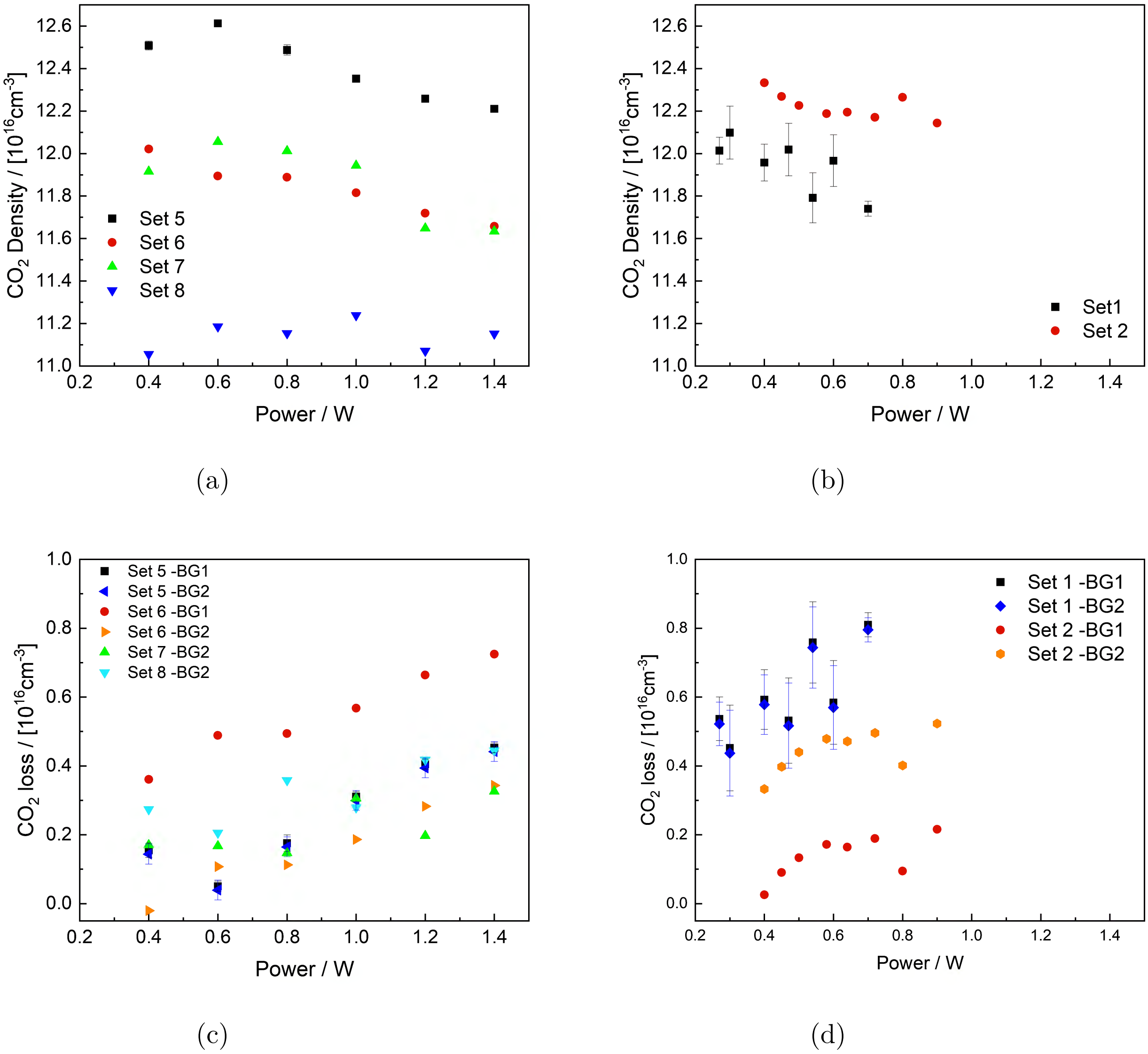

Figure 31: (a) CO_2 densities measured on different days as function of plasma power at a CO_2 admixture of 4975 ppm in ambient air. Set 7 and 8 were done by getting the background after each measurement. (b) CO_2 densities measured on different days as function of plasma power at a CO_2 admixture of 4975 ppm in Helium atmosphere. (c) CO_2 loss as function of plasma power at a CO_2 admixture of 4975 ppm in ambient air. (d) CO_2 loss as function of plasma power at a CO_2 admixture of 4975 ppm in Helium atmosphere.

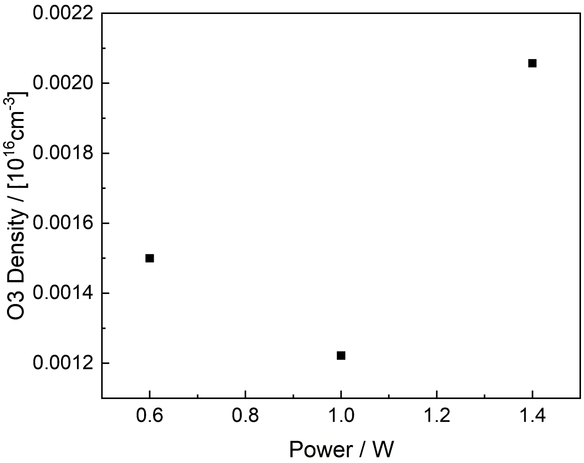

(a)

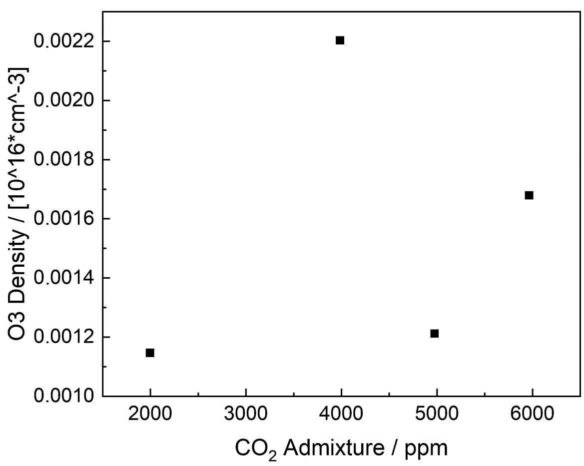

(b)

Figure 32: (a) O_3 densities as function of power in ambient air. (b) O_3 densities as function of admixture in ambient air.

B. Constants

Table 1: Overview of the relevant parameters for the measured species and their calibration species. Adapted from [10]

Species to be measured			**Calibration species**		
Species	Mass amu	E_i eV	Species	Mass amu	E_i eV
CO_2	44	70	CO_2	44	70
CO	28	18	O_2	32	15.5
CO	28	15	O_2	32	15
O_2	32	70	O_2	32	70
O	16	16	Ne	20	25

Table 2: Electron impact ionization cross sections used in this thesis. Adapted from [10]

Species	E_i eV	σ_{EI} cm^2	Ref.
CO	18	$2.54 \cdot 10^{-18}$	[22]
CO	15	$5.1 \cdot 10^{-18}$	[22]
O_2	15.5	$7.30 \cdot 10^{-18}$	[22]
O_2	15	$5.95 \cdot 10^{-18}$	[22]
O	16	$9.9 \cdot 10^{-18}$	[22]
Ne	25	$3.70 \cdot 10^{-18}$	[23]

References

[1]B. E. Mann and R. Motterlini, “CO and NO in medicine”, Chem. Commun., Publisher: The Royal Society of Chemistry, 4197–4208 (2007).

[2]“Carbon monoxide in plasma medicine and agriculture: just a foe or a potential friend?”, Plasma Medicine **8**, 93–120 (2018).

[3]J. Golda et al., “Concepts and characteristics of the COST reference microplasma jet”, Journal of Physics D: Applied Physics **49**, 084003 (2016).

[4]J. Winter, R. Brandenburg and K.-D. Weltmann, “Atmospheric pressure plasma jets: an overview of devices and new directions”, Plasma Sources Science and Technology **24**, Publisher: IOP Publishing, 064001 (2015).

[5]Y. Raizer, *Gas discharge physics* (Springer, Berlin ; New York, 1997), 449 pp.

[6]M. Moravej et al., “Physics of high-pressure helium and argon radio-frequency plasmas”, Journal of Applied Physics **96**, 7011–7017 (2004).

[7]A. A. Fridman, *Plasma chemistry* (Cambridge University Press, Cambridge, 2008).

[8]J. Gross, *Mass spectrometry: a textbook*, 1st ed. (Springer, 2004).

[9]S. Große-Kreul, “Mass spectrometry of ions from atmospheric pressure plasmas”, (2016).

[10]G. Willems, “Reaction chemistry in non-equilibrium atmospheric pressure plasmas”, 158.

[11]J. Held, *Advanced lab course 408: ion velocity distributions in high power impulse magnetron sputtering plasmas*, June 7, 2021.

[12]J. Benedikt, A. Consoli, M. Schulze and A. von Keudell, “Time-resolved molecular beam mass spectrometry of the initial stage of particle formation in an Ar/He/C2H2 plasma.”, The journal of physical chemistry. A **111 42**, 10453–9 (2007).

[13]S. Kelly, J. Golda, M. M. Turner and V. S.-v. d. Gathen, “Gas and heat dynamics of a micro-scaled atmospheric pressure plasma reference jet”, Journal of Physics D: Applied Physics **48**, Publisher: IOP Publishing, 444002 (2015).

[14]R. Pearse and A. Gaydon, *The identification of molecular spectra* (Chapman and Hall ; Wiley, London, New York und 1976, 1976).

[15]M. Ceppelli, T. P. W. Salden, L. M. Martini, G. Dilecce and P. Tosi, “Time-resolved optical emission spectroscopy in CO_2 nanosecond pulsed discharges”, Plasma Sources Science and Technology **30**, Publisher: IOP Publishing, 115010 (2021).

[16]P. Erman et al., “Direct determination of the ionization potential of CO by resonantly enhanced multiphoton ionization mass spectrometry”, **215**, 173 (1993).

[17]D. Lide(Editor), *Handbook of chemistry and physics* (CRC Press, 1992).

[18]R. Locht and J. Momigny, “Mass spectrometric study of ion-pair processes in diatomic molecules: H2, CO, NO and O2”, International Journal of Mass Spectrometry and Ion Physics **7**, 121–144 (1971).

[19]C. Stewig, T. Urbanietz, L. Chauvet, M. Böke and A. von Keudell, “Dedicated setup to isolate plasma catalysis mechanisms”, Journal of Physics D: Applied Physics **54**, 134005 (2021).

[20]C. Stewig, S. Schüttler, T. Urbanietz, M. Böke and A. von Keudell, “Excitation and dissociation of CO_2 heavily diluted in noble gas atmospheric pressure plasma”, Journal of Physics D: Applied Physics **53**, 125205 (2020).

[21]T. Trickl, E. F. Cromwell, Y. T. Lee and A. H. Kung, “State-selective ionization of nitrogen in the $X^2\Sigma_g^+ \mathrm{v}_+ = 0$ and $\mathrm{v}_+ = 1$ states by two-color (1+1) photon excitation near threshold”, J. Chem. Phys. **91**, Publisher: American Institute of Physics, 6006–6012 (1989).

[22]*Springermaterials : the landolt-börnstein database.* eng, Berlin, 1900.

[23]E. Brook, M. Harrison and A. Smith, “Measurements of the electron impact ionisation cross sections of He, C, O and N atoms”, Journal of Physics B: Atomic and Molecular Physics **11**, 3115 (2001).

[24]A. von Keudell, *Vorlesungsskript: Einführung in die Plasmaphysik*, 2021.

Acknowledgements

Lastly I want to express my gratitude to everyone that has been helping me during the course of this thesis. I owe special thanks to

- Jun.-Prof. Dr. Judith Golda for giving me the opportunity to work on this project and always being there to help and to provide guidance
- Dr. Laura Chauvet for always being extremely supportive and guiding me along every step of the way of creating this thesis
- Claire Douat and Eloise Mestre for graciously hosting us during our research visit in Orleans
- everyone at the EP2 institute for creating an extremely supportive, caring and overall fun work environment

Most of all I want to thank my family and friends for not only supporting me during the creation of this thesis, but throughout all of my studies.

Auf gute Freunde!